TALPID3 controls centrosome and cell polarity and the human ortholog KIAA0586 is mutated in Joubert syndrome (JBTS23)

TALPID3 controls centrosome and cell polarity and the human ortholog *KIAA0586* is mutated in Joubert syndrome (*JBTS23*)

Louise A Stephen, Hasan Tawamie, Gemma M Davis, Lars Tebbe, Peter Nürnberg, Gudrun Nürnberg, Holger Thiele, Michaela Thoenes, Eugen Boltshauser, Steffen Uebe, Oliver Rompel, André Reis, Arif B Ekici, Lynn McTeir, Amy M Fraser, Emma A Hall, Pleasantine Mill, Nicolas Daudet, Courtney Cross, Uwe Wolfrum, Rami Abou Jamra, Megan G Davey, Hanno J Bolz

DOI: http://dx.doi.org/10.7554/eLife.08077

Cite as: eLife 2015;10.7554/eLife.08077

Received: 13 April 2015
Accepted: 19 September 2015
Published: 19 September 2015

TALPID3 controls centrosome and cell polarity and the human ortholog *KIAA0586* is mutated in Joubert syndrome (*JBTS23*)

Louise A. Stephen[1], Hasan Tawamie[2], Gemma M. Davis[1], Lars Tebbe[3], Peter Nürnberg[4,5], Gudrun Nürnberg[4], Holger Thiele[4], Michaela Thoenes[6], Eugen Boltshauser[7], Steffen Uebe[2], Oliver Rompel[8], André Reis[2], Arif B Ekici[2], Lynn McTeir[1], Amy M. Fraser[1], Emma A. Hall[9], Pleasantine Mill[9], Nicolas Daudet[10], Courtney Cross[11], Uwe Wolfrum[3], Rami Abou Jamra[2,12,13*], Megan G. Davey[1*+], Hanno J. Bolz[6,14*+]

[1]Division of Developmental Biology, The Roslin Institute and R(D)SVS, University of Edinburgh, Easter Bush, Midlothian, UK EH25 9RG

[2]Institute of Human Genetics, Friedrich-Alexander-Universität Erlangen-Nürnberg, Erlangen, Germany

[3]Cell and Matrix Biology, Institute of Zoology, Johannes Gutenberg University (JGU) of Mainz, Germany

[4]Cologne Center for Genomics (CCG) and Center for Molecular Medicine Cologne (CMMC), University of Cologne, Germany

[5]Cologne Excellence Cluster on Cellular Stress Responses in Aging-Associated Diseases (CECAD), University of Cologne, Germany

[6]Institute of Human Genetics, University Hospital of Cologne, Cologne, Germany

[7]Department of Paediatric Neurology, University Children's Hospital of Zurich, Zurich, Switzerland

[8]Institute of Radiology, Friedrich-Alexander-Universität Erlangen-Nürnberg, Erlangen, Germany

[9]MRC Human Genetics Unit MRC IGMM, University of Edinburgh, UK

[10]UCL Ear Institute, London WC1X 8EE, UK

[11]A.T Still University, School of Osteopathic Medicine, 5850 E. Still Circle, Mesa, Arizona, 85206

[12]Centogene AG, Rostock, Germany

[13]Institute of Human Genetics, University Medical Center Leipzig, Leipzig

[14]Bioscientia Center for Human Genetics, Ingelheim, Germany

* equal senior authors

+ Corresponding authors: megan.davey@roslin.ed.ac.uk; hanno.bolz@uk-koeln.de

Short title: *KIAA0586* (*TALPID3*) is mutated in Joubert syndrome

Key words: Joubert syndrome, intellectual disability, *TALPID3*, *KIAA0586*, cilia, ciliopathy, centrosome, cell polarity, centriolar satellites

ABSTRACT

Joubert syndrome (JBTS) is a severe recessive neurodevelopmental ciliopathy which can affect several organ systems. Mutations in known JBTS genes account for approximately half of the cases. By homozygosity mapping and whole-exome sequencing, we identified a novel locus, *JBTS23*, with a homozygous splice site mutation in *KIAA0586* (alias *TALPID3*), a known lethal ciliopathy locus in model organisms. Truncating *KIAA0586* mutations were identified in two additional JBTS patients. One mutation, c.428delG (p.Arg143Lysfs*4), is unexpectedly common in the general population, and may be a major contributor to JBTS. We demonstrate KIAA0586 protein localization at the basal body in human and mouse photoreceptors, as is common for JBTS proteins, and also in pericentriolar locations. We show that loss of *TALPID3* (*KIAA0586*) function in animal models causes abnormal tissue polarity, centrosome length and orientation, and centriolar satellites. We propose that JBTS and other ciliopathies may in part result from cell polarity defects.

INTRODUCTION

Joubert syndrome (JBTS) is a rare ciliopathy characterized by a specific midhindbrain malformation presenting as 'molar tooth sign' on axial MRI. Patients typically have a perturbed respiratory pattern in the neonatal period and pronounced psychomotor delay. Depending on the genetic subtype, there may be additional retinal degeneration, nephronophthisis, liver fibrosis and skeletal abnormalities (such as polydactyly). JBTS is genetically heterogeneous, with recessive mutations reported in more than 20 genes encoding proteins related to the function of cilia and associated structures (1, 2).

Cilia are axoneme-based organelles which protrude into the extracellular milieu, anchored to the cell by a modified centriole (basal body). They are present in virtually every cell type (3). Non-motile 'primary' cilia play essential roles in mechanotransduction, chemosensation and intracellular signal transduction, including Hedgehog (Hh), PDGFα and WNT pathways, in embryonic development and adult tissue homeostasis (4). In addition, highly modified and specialized cilia constitute the light-sensitive outer segments of retinal photoreceptor cells. Dysfunction of cilia, centrioles of basal bodies and centrosomes can lead to a spectrum of developmental single- or multi-organ disorders termed "ciliopathies" (5).

KIAA0586 (*TALPID3*; MIM #610178, MIM #000979-9031) is essential for vertebrate development and ciliogenesis. The KIAA0586 (TALPID3) protein is localized at the centrosome in human, chicken, mouse and zebrafish cells (6-8), and in particular at the distal end of the mother centriole – the basal body of cilia (9). In model organisms, *KIAA0586* null mutations cause failure of basal body docking and loss of cilia, leading to early embryonic lethal phenotypes (6, 10-12). KIAA0586 (TALPID3) binding partners include PCM1, Cep120 and CP110, which interact with a known JBTS protein, CEP290 (13).

Here, we report three JBTS families with loss-of-function mutations in *KIAA0586*. Using animal models, we demonstrate that *TALPID3* (*KIAA0586*) is not only essential for

transduction of Hedgehog signaling but plays an important role in centrosomal localization, orientation and length. Finally, and beyond its established requirement for ciliogenesis, *TALPID3* (*KIAA0586*) plays a key role in cell and tissue polarity.

METHODS

Patients

Blood samples for DNA extraction were obtained with written informed consent. All investigations were conducted according to the Declaration of Helsinki, and the study was approved by the institutional review board of the Ethics Committees of the University of Erlangen-Nürnberg, the University of Bonn, and the University Hospital of Cologne.

Genetic analysis of human JBTS families

In accordance with the Human Gene Nomenclature Committee (HGNC), we have used *KIAA0586*/KIAA0586 for designation of the human gene and protein, respectively. In accordance with the Chicken Gene Nomenclature Committee (CGNC), we use *TALPID3*/TALPID3 for designation of the chicken gene and protein, respectively. Although the current gene symbol for the mouse gene is *2700049A03Rik* (protein: 2700049A03RIK), we use *Talpid3*/Talpid3 as the gene and protein names, respectively. Where we refer to a generic conclusion on the function of the orthologs of *KIAA0586*, we use *KIAA0586*. As in previous publications, the chicken model is referred to as *talpid*^{3}, and the mouse model is referred to as *Talpid3*$^{-/-}$. The nomenclature of human *KIAA0586* mutations refers to reference sequence NM_001244189.1 (corresponding protein: NP_001231118.1). The Exome Aggregation Consortium (ExAC) database (Cambridge, MA, USA; http://exac.broadinstitute.org), which aggregates numerous databases including the current versions of the Exome sequencing project (ESP, (14)) and the Thousand Genomes Project (TGP, (15)) was last accessed on July 11, 2015 for presence and frequency of identified variants in healthy individuals.

105 Family 1: Genotyping and homozygosity mapping were performed in Family 1 (MR026) as
106 previously reported (16). DNA from patient MR026-01 underwent exome capture and whole-
107 exome sequencing (WES) using the SureSelect Human All Exon 50 Mb Kit (Agilent
108 technologies, Santa Clara, USA) and a SOLiD4 instrument (Life Technologies, Carlsbad,
109 USA) as described previously (17). Of the targeted regions, 73.2% were covered at least 20x,
110 and 83.4% at least 5x. To validate the results, we also conducted WES in the likewise
111 affected sibling, MR026-04, analogous to previously described disease gene identification
112 approaches (18, 19). 96% of the target sequence were covered at least 20x.
113 Family 2: Samples from the index patient, MD1, and her parents underwent WES at GeneDX
114 (Gaithersburg, MD).
115 Family 3: WES and mapping of reads for the index patient (G2) and both parents were
116 carried out as previously described (20, 21). In brief, filtering and variant prioritization was
117 performed using the varbank database and analysis tool (https://varbank.ccg.uni-koeln.de) of
118 the Cologne Center for Genomics. In particular, we filtered for high-quality (coverage >15-
119 fold; phred-scaled quality >25), rare (MAF (minor allele frequency) ≤0.001) variants (dbSNP
120 build 135, the 1000 Genomes database build 20110521, and the public Exome Variant
121 Server, NHLBI Exome Sequencing Project, Seattle, build ESP6500). To exclude pipeline-
122 related artifacts (MAF≤0.01), we filtered against variants from in-house WES datasets from
123 511 epilepsy patients. The Affymetrix genome-wide Human SNP Array 6.0 utilizing more
124 than 906,600 SNPs and more than 946,000 copy number probes was used for genome-wide
125 detection of copy number variations in patient G2. Quantitative data analyses were performed
126 with GTC 3.0.1 (Affymetrix Genotyping Console) using HapMap270 (Affymetrix) as
127 reference file. In the index patient (G2), all coding *KIAA0586* and *KIF7* exons were Sanger-
128 sequenced in search of a second mutation. In addition, we amplified and sequenced all
129 *KIAA0586* exons from cDNA (derived from whole blood mRNA, PAXgene Blood RNA

Tube, PreAnalytiX, Hombrechtikon, Switzerland) in search of potential hints of aberrant splicing due to extra-exonic variants. Continuous PCR-amplification of *KIF7* exons from whole-blood mRNA was not successful. The sample of patient G2 was analyzed by genome-wide CGH (Affymetrix 6.0 SNP array) to exclude structural alterations adjacent to or within *KIAA0586*, *KIF7*, *CEP41*, *KIF14* or *WDPCP*. Confirmation of the identified mutations and segregation analyses were carried out by Sanger sequencing.

RT-PCR

In Family 1, we isolated mRNA using the RNeasy kit (QIAGEN, Hilden, Germany) from lymphoblastoid cell lines that have been established based on standard protocols from patients MR026-01 and MR026-04. We transcribed mRNA to cDNA using SuperScriptII reverse transcriptase and random primers (Invitrogen). To test if the *KIAA0586* mutation c.2414-1G>C impairs splicing, we used two pairs of primers (*KIAA0586*_exprF1, 5′-TCCATCTCCTAAGTCCAGACCAC-3′ and *KIAA0586*_expR1, 5′-TCCAAGTTTGCACAGGAGG-3′, located in exons 16 and 19, and *KIAA0586*_exprF2, 5′-TCAGGTACATTGGAAGGTCATC-3′ and *KIAA0586*_expR2, 5′-AACTGGCGGAAATGGAGG-3′, located in exons 17 and 21; NM_001244189.1), and standard PCR methods. Electrophoresis on standard agarose gel followed by cutting out the DNA bands, purifying the DNA using QIAquick gel extraction kit (QIAGEN), and Sanger sequencing were performed.

Animal models

Eggs were obtained from *talpid*^{3} flock (MG Davey; *talpid*^{3} chicken lines are maintained at the Roslin Institute under UK Home Office license 60/4506 [Dr. Paul Hocking], after ethical review). Mice were maintained at the Human Genetics Unit, Western General, Edinburgh,

under UK Home Office license PPL 60/4424 [Ian Jackson]. The *Talpid3*$^{+/-}$/*Kif7*$^{+/-}$ line was produced by crossing of the previously described *Talpid3*$^{+/-}$ knockout mouse line (10) and the reported *Kif7*$^{+/-}$ mouse line (22). Animal experiments carried out at the JGU Mainz corresponded to the statement of the Association for Research in Vision and Ophthalmology (ARVO) as to care and use of animals in research. Adult mice were maintained under a 12 hour light–dark cycle, with food and water ad libitum.

Incubation and dissection of animal models

Chicken eggs from *talpid*^{3} flock were incubated at 38°C until 12 days at the latest, staged as per Hamburger and Hamilton 1951 (23), dissected into cold PBS and fixed in 4% PFA/PBS. Mouse timed matings were established between *Talpid3*$^{+/-}$ mice (10) and *Kif7*$^{+/-}$ mice (22) and confirmed by vaginal plug. Pregnant females were sacrificed at day 10 of pregnancy, embryos dissected and used to make mouse embryonic fibroblasts or between day 12-16 of pregnancy and embryos were dissected in cold PBS, decapitated and fixed immediately in 4% PFA, or pups were sacrificed between 7-21 days after birth by lethal injection. Brains were dissected into 4% PFA/PBS.

Chicken and mouse genotyping

Embryos used in comparisons were dissected as family groups and genotyped after analysis. Tissues were collected on dissection, lysed in 10 mM Tris (pH8), 10 mM EDTA (pH 8), 1 % SDS, 100 mM NaCl and 20 mg/ml proteinase K at 55°C overnight before DNA extraction using Manual Phase Lock Gel Tubes (5 Prime) for phenol/chloroform extraction. For chicken *TALPID3*, sequencing primers used were 5'-TCATTTCATTAGCTCTGCCG-3' (forward) and 5'-CCATCAAACCAACAGCTCAG-3' (reverse). For mouse *Talpid3*, PCR primers were 5'-TGCCATGCAGGGATCATAGC (forward), 5'-GAGCACACTGGAGGAAAGC-3'

(reverse) and 5'-GAGACTCTGGCTACTCATCC-3', 5'-CCTTCAGCAAGAGCTGGGGAC-3', respectively. For mouse *Kif7*, PCR primers were- 5'-CACCACCATGCCTGATAAAAC-3' (P1 forward), 5'-CTATCCCCAATTCAAAGTAGAC-3' (P1 reverse), 5'-CCAAATGTGTCAGTTTCATAGC-3' (P2 forward), 5'-TTCTCACCCAAGCTCTTATCC-3' (P2 reverse).

Histology

Fixed samples from mouse brain and chicken legs were embedded in paraffin, sectioned and stained in haematoxylin and eosin as described previously (24).

Wholemount RNA *in situ* hybridisation

Mouse and chicken embryos were rehydrated through a methanol gradient and *in situ* hybridization carried out for chicken β-catenin (codons 1–127) as previously described (25).

***In ovo* knockdown of *Kif7* in chicken**

The following *Kif7* sequences were targeted for knockdown: Target 1: TTATCGACGAGAACGACCTCAt, Target 2: cATCCAGAACAAAGCGGTGGTG, Target 3: gTCCTCTAACACTAAGAACATT, Target 4: gACAGATGACATAGTCCGTGTG to which 22mer sequences were designed in Genscript and cloned into pRFPRNAiC (26) (Dundee Cell Products, UK). Embryos were electroporated at stage 12HH (as described (7)), observed for RFP expression at stage 24HH, fixed and prepared for sectioning and immunohistochemistry at stage 22HH as below. Tissue from embryos was collected and genotyped.

205 **Cell culture and immunocytochemistry**

206 Mouse embryonic fibroblasts (MEFs) were prepared from E10.5 eviscerated and decapitated
207 embryos. Cells were dissociated in trypsin/versin and maintained to passage 2 as per (27) and
208 serum removed from media for 48 hours to induce ciliogenesis. RPE1 cells (ATCC) were
209 grown in DMEM-F12, 10% FCS Gold, 50 µl hygromycin, 5 ml L-glut. IMCD3 (mouse inner
210 medullary collecting duct cells) cells were grown in DMEM-F12 10% FCS. To induce
211 ciliogenesis, RPE1 and IMCD3 cells were starved in DMEM:F12 or Opti-MEM I (Life
212 Technologies) for 72 h. Cells were fixed with methanol at -20°C for 2-5 minutes. After
213 washing in PBS, cells were immunolabeled with polyclonal antibodies against acetylated
214 tubulin (Sigma-Aldrich T7451), pericentrin-2 (Santa Cruz sc-28145) and KIAA0586 (Atlas
215 HPA000846) before incubation with appropriate secondary antibodies conjugated to Alexa
216 488 (Molecular Probes A21206), CF 568 (Biotrend 20106-1), and CF 640 (Biotrend 20177)
217 and with DAPI (Roth 6335.1).
218
219 **Immunohistochemistry**

220 Eyes from a healthy human donor (#199-10; 56 years of age, dissection 29 hours post
221 mortem) were obtained from the Department of Ophthalmology, University Hospital of
222 Mainz, Germany, according to the guidelines of the declaration of Helsinki. After sacrifice,
223 eyeballs from adult C57BL/6J mice were dissected, cryofixed in melting isopentane,
224 cryosectioned and immunostained as previously described (28). Cryosections were incubated
225 with monoclonal antibodies to centrin-3 as a molecular marker for the ciliary apparatus of
226 photoreceptor cells as previously characterized (29), and polyclonal antibodies against
227 KIAA0586 (Atlas HPA000846). Washed cryosections were incubated with appropriate
228 antibodies conjugated to Alexa 488 (Molecular Probes A21206) and Alexa 568 (Molecular
229 Probes A11031)) in PBS with DAPI (Roth 6335.1) to stain the nuclear DNA and mounted in

Mowiol 4.88 (Hoechst, Germany). Specimens were analyzed in a Leica DM6000B deconvolution microscope (Leica, Germany). Image contrast was adjusted with Adobe Photoshop CS using different tools including color correction. For section immunocytochemistry on chicken tissue, chicken embryos were dissected into PBS, fixed, sectioned and stained as described (11), except for CEP164, in which an antigen retrieval step was undertaken (incubation in 0.1% BME/PBS for 5 min., incubation in 55°C PBS for 4 hours). For bone sections, legs were dissected at E12. For immunocytochemistry, cells were fixed as above. Antibodies were used against: acetylated α-tubulin (Sigma-Aldrich T7451), γ-tubulin (Sigma-Aldrich T5192; T5326), TGN46 (Abcam ab16059), PCM1 (Abcam ab72443), AZI1 (kind gift of Jeremy Reiter, UCSF), centrin-3 (29), KIAA0586 (Atlas HPA000846, ProteinTech 24421-1-AP), CEP164 (ProteinTech 22227-1) RFP (Life Technologies R10367), GFP (Life Technologies A-21311), Pax7 (Developmental Studies Hybridoma Bank (DSHB)), ISLET1 (DSHB), NKX2.2 (DSHB), Phalloidin (Life Technologies A12379), Anti-mouse (Life Technologies A11017), anti-rabbit (Life Technologies A21207). Imagining was undertaken on a Zeiss LSM 710 or a Nikon Air confocal microscope or Leica DMLB.

Conventional transmission electron microscopy (TEM)

Chicken embryos were dissected into PBS at 8 days of incubation, avoiding contamination with yolk, heads were removed and placed into 4% PFA, 2.5% glutaldehdye in 0.1 M cacodylate buffer. The choroid plexus was immediately removed and placed into fresh fixative (as previous) for 24 hours. Tissue was prepared and visualized for TEM as described previously (30), and axoneme/basal body structure was compared to what was observed and reported previously (31).

Immunoelectron microscopy analysis

Anti-KIAA0586 antibody (Atlas HPA000846) was used for pre-embedding labeling in mouse retinas as previously described (32, 33). Ultrathin sections were cut on a Leica Ultracut S microtome and analyzed with a Tecnai 12 BioTwin transmission electron microscope (FEI, The Netherlands). Images were obtained with a charge-coupled device SIS Megaview3 SCCD camera (Surface Imaging Systems, Herzogenrath, Germany) and processed with Adobe Photoshop CS.

Cell polarization and cilia length measurements

Angles of proliferation, migration, orientation and localization were calculated using Axiovision Angle3 software, and cilium length was measured using Zen software (Zeiss, Oberkochen, Germany). Scratch assays were carried out in *wildtype* and *Talpid3*$^{-/-}$ MEFs grown to confluence and serum starved (DMEM + 0.5% FCS) for 48 hours with a p10 pipette tip. Medium was then renewed and MEFs incubated for four hours before fixation in ice-cold methanol prior to immunofluorescence. Angles of orientation were then taken as a measurement of the angle from the centre of the nucleus, through the centre of the leading edge (towards the wound, identified by phalloidin staining for F-actin) and again through the centre of the Golgi apparatus (identified by TGN46 antibody staining). Tiled Z stacks of the scratch/wound were analyzed for greater accuracy (Figure 3O).

The expected orientation of the stereocilia of the basilar papilla hair cells were taken as being at 90° to the abneural edge of the basilar papilla. The angle of orientation was taken by drawing a line through the cell perpendicular to the abneural edge and a second from the centre of the cell, intersecting with both the perpendicular line and centre of the actin bundle. The internal angle was taken to be the angle by which cell orientation deviated from the expected. Cilium length was measured using Zen software (Zeiss, Oberkochen, Germany).

RESULTS

Clinical description of patients with *KIAA0586*-associated JBTS

The diagnosis of JBTS was based on the presence of a molar tooth sign in all three families. Family 1 (Figure 1A) is a consanguineous Kurdish family from northeast Syria. The two affected siblings were examined at the age of 6 years and 10 months (MR026-01) and 2 years and 2 months (MR026-04), respectively. Pregnancy, delivery, and birth parameters of both children were unremarkable. In the neonatal period, both were hypotonic and weepy. Motor and speech development in MR026-01 were delayed, and his IQ was estimated to be between 50 and 70. Further symptoms were severe myopia, scoliosis, brachydactyly, distinct facial characteristics, and recurrent febrile seizures. Height was reduced (108 cm, -2.6 SD), weight was normal (22 kg, -0.27 SD), and head circumference was increased (57 cm, +2.3 SD). MR026-04 had not reached any milestones, and at the age of 7 years, she was wheelchair-bound. Cognitive abilities were weaker than in her brother, with an IQ estimated to be below 35. MR026-04 had similar physical characteristics as her brother, severe muscular hypotonia, prolonged and therapy-resistant seizures since the age of 14 months, and hypothyroidism. At the time of examination, her height was 91 cm (1 SD), weight was 11.5 kg (-0.7 SD), and there was macrocephaly (head circumference of 59 cm, +8 SD).

Family 2 (Figure 1B) is of North American origin. Patient MD1 was born at 34 3/7 weeks gestation following preterm premature rupture of membranes at 26 weeks. At birth, patient MD1 was found to have cardiac defects including a patent ductus arteriosus (PDA), patent foramen ovale (PFO) and a 3/6 ventricular septal defect (VSD) causing persistent pulmonary hypertension 24 hours after birth. The PDA and PFO resolved, and VSD was at 2/6 within 22 days. At 7 months, MD1 was found to have a superior vena cava duplication. At 2 years of age, MD1 has hypotonia which inhibits motor actions, although she can crawl proficiently,

uses sign language and single words, and can self-feed by hand and with utensils. In addition, she had type I bilateral Duane syndrome with no abduction in either eye, narrowing of the palprebal fissure of the inturned eye, was farsighted, had thin tooth enamel, held her jaw sideways in a cross-bite pattern, and had long fingers with a slight clinodactyly of the 5th finger. She had a broad forehead, arched eyebrows, ptosis of the right eye, and a triangle shaped mouth. Her receptive language was good. There was intermittent hyperpnea/apnea during awake periods. Patient MD1 had no liver, kidney, or eye abnormalities at 2 years of age.

Family 3 (Figure 1C) is of German origin: Patient G2 displayed a relatively mild JBTS phenotype with developmental delay and behavioral abnormalities, but no dysmorphic signs of renal, retinal, skeletal or liver systems. His symptoms were described previously (Figure 1C, (34)).

Mutations of *KIAA0586* cause JBTS

We have identified *KIAA0586* mutations in three JBTS families (Figure 1A-D). Genome-wide SNP genotyping in Family 1 identified eight homozygous chromosomal candidate regions with a total range of 67.1 Mb. By WES, the homozygous mutation c.2414-1G>C in intron 17, affecting the invariant consensus of the exon 18 acceptor splice site, was found in the index patient, MR026-01, and his affected sister, MR026-04. Segregation analysis in the family was compatible with causality (Figure 1A). The mutation was absent from 372 healthy Syrian controls, including 92 of Kurdish origin, and not listed in the ExAC database.

In patient MD1 from Family 2, WES identified compound heterozygosity for the *KIAA0586* mutations c.428delG (p.Arg143Lysfs*4; rs534542684; MAF of 0.39% in ExAC db) and c.2512C>T (p.Arg838*), each inherited from a healthy parent (Figure 1B), and both resulting in premature stop codons. Because the coiled coil domain, which is essential for KIAA0586

function in mouse, chicken and zebrafish (residues 531-571 and residues 497-530 in human and chicken KIAA0586, respectively; Figure 1E), would be lost in a truncated protein derived from the c.428delG mutation, we consider it a loss-of-function mutation (as is the case for the *talpid*^{3} chicken mutation which introduces a frameshift 3' to c.428 in the chicken ortholog, Figure 1E). Like the *Talpid3*/*TALPID3* null mutations in mouse and chicken, c.428delG is clearly recessive because the father of the patient is a healthy carrier. The c.2512C>T (p.Arg838*) mutation is predicted to lead to nonsense-mediated decay (NMD) or a truncated protein, but with preservation of the essential coiled coil domain.

The simplex patient of Family 3, G2, was a known carrier of a heterozygous N-terminal frameshift mutation in exon 3 of the *JBTS12* gene *KIF7*, c.811delG (p.Glu271Argfs*51) (34). WES of the family trio (patient G2 and his parents) additionally identified the c.428delG (p.Arg143Lysfs*4) mutation in *KIAA0586*, in the patient (Figure 1C). We hypothesized that disease in patient G2 could be due to biallelic mutations either in *KIF7* (*JBTS12*) or in *KIAA0586* (*JBTS23*), assuming that the "missing mutation" has escaped detection by sequencing due to an extra-exonic localization. Genome-wide CGH (Affymetrix 6.0 SNP array) did not reveal structural alterations adjacent to or within *KIF7* (34) or *KIAA0586*, thereby largely excluding a large deletion or duplication. PCR amplification and subsequent sequencing of *KIAA0586* exons from cDNA did not reveal aberrant splicing as a potential hint for a deep intronic splice site mutation. Because *KIF7* and *KIAA0586* both encode modulators of GLI processing and c.428delG$_{KIAA0586}$ and c.811delG$_{KIF7}$ likely represent recessive loss-of-function mutations, we investigated the possibility of a potential epistatic effect predisposing to JBTS. No such interactions were identified in mouse and chicken experiments (details are fully described in Figure 1- figure supplement 1). Therefore, unidentified mutations are likely to be involved, either mutations in *KIF7*, *KIAA0586* (e.g. deep intronic mutations or alterations in non-coding regulatory regions which would both not

be covered by WES), or biallelic mutations in another (yet unknown) JBTS gene. WES revealed further heterozygous missense variants in three known recessive ciliopathy genes in patient G2 (Figure 1C), all affecting evolutionarily conserved residues of the respective proteins: 1. c.536G>A (p.Arg179His, rs140259402; MAF of 0.001647% in ExAC db) in *CEP41*, the gene associated with *JBTS15* (35). 2. c.3181A>G (p.Ile1061Val; MAF of 0.01155% in ExAC db) in *KIF14*, a gene associated with a lethal fetal ciliopathy phenotype (36). 3. c.1333G>C (p.Ala445Pro, rs61734466; MAF of 0.6609% in ExAC db) in *WDPCP*, the gene associated with Bardet-Biedl syndrome type 15 (*BBS15*), and a putative contributor to Meckel Gruber syndrome (37).All variants were of paternal origin and rare in the general population except the *WDPCP* allele, which had been maternally inherited and which has been annotated homozygously in five healthy individuals (ExAC db), indicating that this is a benign variant. Genome-wide CGH (Affymetrix 6.0 SNP array) did not show structural alterations adjacent to or within *CEP41*, *KIF14* or *WDPCP*. In addition, we searched the WES data of patient G2 for heterozygous putative loss-of-function (that is, truncating) variants in genes with documented ciliary function. This revealed a paternally inherited frameshift variant, c.206_207insA (p.Ser70Valfs*3), in *PLA2G3*, the gene encoding phospholipase A2. In a functional genomic screen, PLA2G3 was found to be a negative regulator of ciliogenesis and ciliary membrane protein targeting (38). The p.Ser70Valfs*3$_{PLA2G3}$ variant is relatively common, but has not been documented in homozygous state in healthy individuals (MAF of 0.4060 in ExAC db).

We also filtered for known JBTS genes carrying at least two rare variants in patient G2, but we did not identify such a constellation. When applying this to all genes captured in the WES approach, there was also no potentially causative double heterozygosity in a gene of known or probable ciliary function. Filtering for homozygous rare and likely pathogenic variants was negative, compatible with lack of consanguinity in the parents of patient G2.

Consequences of the *KIAA0586* mutation c.2414-1G>C on mRNA level

The c.2414-1G>C mutation affects the invariant consensus of the acceptor splice site of exon 18. RT-PCR and Sanger sequencing of the fragments amplified from cDNA revealed three aberrant splicing products due to usage of alternative exonic acceptor splice sites at AG motifs within exon 18 and due to skipping of exon 18 (Figure 1D,E): a 13-bp deletion that results in a premature termination codon (alternative acceptor splice site at c.2425/2426AG), a 108-bp in-frame deletion (alternative acceptor splice site at c.2520/2521AG), and a 188-bp deletion due to skipping of exon 18 that results in a premature stop codon. These aberrant transcripts were present in the cDNA from both patients, but not in the cDNA of a healthy control individual (Figure 1D). The mutant mRNA molecules are likely to be degraded by NMD. If the mutant transcripts were stable, the essential coiled coil domain (Figure 1E), which mediates centrosomal localization and function of KIAA0586 protein (7, 8), would be preserved.

KIAA0586 localizes to the basal body of cultured cells and photoreceptor cells of human and mouse retina

KIAA0586 is a centrosomal protein and localizes to the basal body and the adjacent centriole of primary cilia in human RPE1, IMCD3 cells (Figure 2A) and other cell types (8, 9). Immunofluorescence analysis of the retina of *wildtype* C57BL/6 mice allowed us to allocate KIAA0586 expression to different retinal layers, namely the photoreceptor layer, the outer and inner plexiform layer, and the ganglion cell layer (Figure 2B). Co-staining with the ciliary marker centrin-3 (29) demonstrated KIAA0586 localization in the ciliary region at the joint between the inner and outer segment of photoreceptor cells in cryosections through the mouse retina and the retina of a human donor eye (Figure 2B,C,E). Higher magnification

revealed that KIAA0586 specifically localized at the basal body (mother centriole) and the adjacent centriole as well as between the two centrioles, but not in the connecting cilium of mouse and human photoreceptor cells (Figure 2D,F). These findings were confirmed by immunoelectron microscopy of KIAA0586 labeling on sections through mouse photoreceptor cilia (Figure 2G,H). Immunostaining was found at centrioles and in the pericentriolar region in the apical inner segment of photoreceptor cells. The spatial distribution of KIAA0586 labeling at the ciliary base of photoreceptor cells is summarized in the scheme of Figure 2J.

Loss of *TALPID3* (*KIAA0586*) causes abnormal tissue and cell polarity

The *talpid*^{3}/Talpid3$^{-/-}$ phenotype in model animals has thus far been attributed to the role of TALPID3 in ciliogenesis and the subsequent loss of Hh-dependent patterning. However, the patients in this study did not display any overt defects typical for impaired Hh signalling such as polydactyly or hypotelorism, which have been described in other JBTS patients (2). *Talpid*^{3} chicken embryos also have polycystic kidneys (7), a phenotype that is frequently ascribed to a loss of oriented cell division (39, 40), as well as cell migration defects (10), which may also occur due to loss of cell polarity (39, 40). To investigate if tissue and cell polarity is impaired by a loss of *TALPID3*, we first examined the patterning of the skin and the inner ear, two highly polarized tissues independent of Hh signaling. At E10, embryonic chicken feather buds express *β-catenin* in an oriented manner, with a larger domain in the anterior part of the bud (Figure 3A,C). While 88% of *wildtype* feather buds at E10 are oriented in this manner (n=117/133), only 21% of stage-matched *talpid*^{3} feather buds were (n=38/179), whilst 22% of *talpid*^{3} buds were oriented in the wrong direction (n=39/179) and 57% had failed to show any orientation of β-catenin expression (n=102/179; Figure 3C'). *Talpid*^{3} feather buds also frequently merged (29% of buds; asterisk, Figure 3B''). Thus, the skin of *talpid*^{3} embryos did not show the characteristic rostral-caudal polarization of *wildtype*

skin. The hair cells (HCs) of the inner ear (known as the basilar papilla (BP) in chicken), have a highly polarized structure determined by the non-canonical Wnt-PCP signaling pathway. In the *wildtype* chicken, as in mouse, individual HCs exhibit an orientated actin-based stereocilia bundle, the apex of which lies at the abneural side of the cell, where within an actin-free 'bare zone', a single kinocilium (a microtubule-based true cilium) forms (arrow, Figure 3D). HCs are frequently used to assess how cell polarity and ciliogenesis are perturbed in mouse mutants (4). The HCs of *talpid*^{3} embryos formed actin filament bundles (curved line, Figure 3E), but no kinocilium, demonstrating that, as with other tissues studied, loss of TALPID3 impairs ciliogenesis. Furthermore, although stereocilia were present in *talpid*^{3} HCs, stereocilia bundles frequently lacked polarity compared to *wildtype* HCs as indicated by either centrally located stereocilia bundles in SEM or actin filaments throughout the cell (*talpid*^{3} n=1086/1195; *wt* n= 258/502; Figure 3D,E,F,G,L). Orientation of the polarized stereocilia bundles that did form in *talpid*^{3} HCs, was also abnormal (Figure 3E,G,N). The orientation of stereocilia was determined in relation to their position to the abneural side of the BP (Figure 3F,G,M). 73% of stereocilia of *wildtype* cells (n=244) were oriented within 40° of the expected angle (90°, compared to 38% of *talpid*^{3} cells (n=237; Figure 3 M'). Thus, *talpid*^{3} HCs showed disrupted polarity.

Loss of *TALPID3* causes abnormal intracellular organization

Loss of *TALPID3* prevents basal body docking (7), which we have previously suggested to be due to failure of centrosome migration (12). The migration and subsequent localization and docking of the centriole is crucial to establish polarity and placement of the actin bundle in the HC (41), and we therefore hypothesized that disturbed cell polarity may result from defective centrosome migration in *talpid*^{3} HCs. Using antibodies against γ tubulin to determine the localization of the centriole within the actin-negative abneural bare zone in the

HCs, 95% of *wildtype* HCs exhibited a basal body (centrosome) within the abneural bare zone (n=632 from 7 samples, Figure 3H,J,N). In contrast, only 49% of *talpid*^{3} cells exhibited a centriole within the bare zone (either abneural or abnormally polarized; n=219 from 6 samples. Figure 3I,K,N), thus demonstrating that the intracellular organization of *talpid*^{3} cells was frequently abnormal. Furthermore, and in agreement with the failure of correct polarization of the stereocilia, centrioles were frequently observed on the neural side of *talpid*^{3} HCs (Figure 3Kii). We conclude that failure of centriolar migration in *talpid*^{3} cells results in abnormal cell polarization and stereocilia formation in HCs. Because 49% of *talpid*^{3} cells did exhibit a centriole correctly localized yet ciliogenesis was completely disrupted, the failure of ciliogenesis may not only be due to impaired centriolar migration.

Directional cell migration is also intimately linked to the localization of the centrosome between the leading edge of the migrating cell and the Golgi apparatus. *Talpid3*$^{-/-}$ MEFs show abnormal cell migration (10), and we therefore examined if the orientation of the Golgi apparatus to the leading edge of migrating cells was also disrupted by a loss of *Talpid3* in mouse, in an *in vitro* scratch assay (Figure 3O,P). The angle between the leading edge and Golgi was taken as the angle of orientation, with an angle of 0° suggesting perfect alignment of the Golgi to the leading edge of the migrating cell (Figure3Q). The angle of orientation was within 40° in 69% of *wildtype* cells and 55% of *talpid3*$^{-/-}$ cells, whilst 20% of *talpid3*$^{-/-}$ cells exhibited orientation angles greater than 60° compared to 11% of *wildtype* cells (Figure 3Q'; *wildtype* cells=132, *talpid3*$^{-/-}$ cells=117 from two experiments; Figure 3O-Q), suggesting a reduction in intracellular polarization of the Golgi apparatus to the leading edge in the *Talpid3*$^{-/-}$ MEFs (Figure 3O,P). Thus, KIAA0586 (TALPID3) plays an essential role in the internal organization and polarization of cells, likely through its action on the centrosome.

Abnormalities of intracellular organization, centriole maturation and centriolar satellite dispersal in the neuroepithelium

JBTS primarily affects the brain of the patients. The choroid plexus is a highly polarized multiciliated neuroepithelium in which we have previously shown, as now in HCs, a failure of centrosome migration in *talpid*^{3} mutant chickens (12). To determine if *talpid*^{3} mutant neuroepithelia exhibits cell polarity defects, we examined the intracellular organization of choroid plexus cells in E8 *talpid*^{3} mutant chickens. *Wildtype* choroid plexus cells exhibited a distinctive polarization with an apical, centriolar zone (CZ, Figure 4A) above a separate zone of mitochondria (MZ, Figure 4A); the most apical mitochondria were found an average of 7 μm from the apical surface (Figure 4C). In contrast, the mitochondria in *talpid*^{3} choroid plexus are found in the most apical zone, an average of 3 μm from the apical surface (m, Figure 4B), and centrioles are present throughout the cell (asterisk in Figure 4B). We conclude that the neuroepithelium has an abnormal intracellular organization of centrosomes and mitochondria and therefore, like the HCs and migratory fibroblasts, is not correctly polarized. Although we have previously suggested that a failure of centrosome migration to the apical surface is the primary reason that cilia fail to form (12) our analysis of the HCs suggest an additional requirement for TALPID3 during ciliogenesis, independent of the centriole migration. We therefore investigated the maturation of the mother centriole, crucial for the basal body to dock to the membrane and initiate ciliogenesis. Subdistal appendages were identified in approximately 40% of *wildtype* and *talpid*^{3} centrioles (*wt* n=35, *talpid*^{3} n=48, Figure 4D,E,G), whereas distal appendages were noted in 28% of *wildtype* centrioles and only 6% of *talpid*^{3} centrioles (Figure 4D-G). To determine if there was a loss of distal appendages, we examined localization of CEP164, a protein known to localize to the distal appendages of the mature mother centriole, the basal body. CEP164 localized correctly at the mother centriole and not at the sister centriole, in both *wildtype* and *talpid*^{3} cells of the

504 neuroepithelium and fibroblasts (Figure 4H-M). However, CEP164 puncta were smaller,
505 disorganized and frequently orientated away from the apical cell surface in *talpid*^{3} cells
506 (Figure 4K,L). This confirmed our previous EM analysis (7) and data in this study, which
507 demonstrated that centrioles frequently failed to migrate or orientate correctly in *talpid*^{3} cells.
508 Smaller sized CEP164 puncta also suggested that distal appendages were not formed
509 normally in *talpid*^{3} cells. As abnormal or absent distal appendages can result in elongation of
510 the centriole due to improper capping, centriolar length was studied in *wildtype* and *talpid*^{3}
511 choroid plexus cells (Figure 4N-Q). Centrioles in *wildtype* tissue were on average 0.7 µm in
512 length compared to 0.9 µm in the *talpid*^{3} chicken, suggesting that *talpid*^{3} centrioles may
513 indeed fail to undergo complete maturation and are subsequently elongated (Figure 4R).
514 In human cells, KIAA0586 is also required for centriolar satellite dispersal (9). Compatible
515 with this, we observed electron-dense condensations around the centrioles in the
516 neuroepithelium of *talpid*^{3} chicken, which were absent from *wildtype* centrioles (basal body;
517 80% of wildtype cell exhibited electron-dense clear area around the centriole, whereas only
518 21% of *talpid*^{3} cells did; *wt* n=35, *talpid*^{3} n=48; Figure 5A,D,G). To determine if these were
519 centriolar satellites, we examined the localization of PCM1, a marker for centriolar satellites.
520 Compared to *wildtype* centrioles (Figure 5B,C), PCM1 puncta were larger around *talpid*^{3}
521 centrioles (Figure 5E,F), possibly reflecting an increase in centriolar satellites. Because we
522 observed KIAA0586 immunostaining around the pericentriolar region (Figure 2G,H), we
523 used the centriolar satellite marker AZI1 in human RPE1 cells to determine if KIAA0586
524 localized to centriolar satellites (Figure 5H-J), but found that KIAA0586 and AZI1 did not
525 colocalize. Thus, as observed in human cell lines, TALPID3 is essential for centriolar satellite
526 dispersal. As TALPID3 protein does not localize to the centriolar satellites, we assume that
527 this is an indirect consequence of *TALPID3* deficiency.
528

529 We conclude that KIAA0586 (TALPID3) is essential for several distinct roles in centriole
530 function, including centriole migration and orientation which can subsequently affect cell and
531 tissue polarity and ciliogenesis, centriole maturation which affects docking of the basal body
532 and ciliogenesis and through an indirect mechanism, centriolar satellite dispersal, which may
533 also affect ciliogenesis.
534

DISCUSSION

JBTS is a genetically heterogeneous condition, caused by mutations in several genes related to the structure and function of cilia (1). Through homozygosity mapping and WES, we identified a novel disease locus (*JBTS23*), defined by mutations in the *KIAA0586* gene, encoding a centrosomal protein (42) (Figure 1), which is supported by simultaneous concurrent studies (43, 44). We used *Talpid3/TALPID3*$^{-/-}$ mouse and chicken models to understand the corresponding pathomechanisms causing the phenotypes of these patients, and discovered centrosome abnormalities and loss of cell polarity.

We confirm localization of KIAA0586 at centrosomal structures at the basal bodies and the adjacent daughter centrioles of primary cilia of mouse and human photoreceptor cells as well as in pericentriolar regions (Figure 2). KIAA0586 has previously been associated with recessive ciliopathy phenotypes in mouse (10, 24), chicken (11, 30) and zebrafish (6). These animal models have either naturally occurring or induced 5' mutations which disrupt an essential coiled coil domain, resulting in loss of protein function, consecutive loss of Hh signaling and early embryonic lethality. The *talpid*^{3} chicken is a thoroughly examined animal model with polydactyly, holoprosencephaly, abnormal neural tube patterning, polycystic kidneys, liver fibrosis, short ribs and endochondral bones with defective ossification (11, 24, 45, 46).

The c.428delG (p.Arg143Lysfs*4) mutation was identified in heterozygous state in patient MD1, *in trans* to a nonsense mutation (Figure 1B), and in a patient G2 who is also heterozygous for a *KIF7* (*JBTS12*) frameshift mutation and variants in three other known ciliopathy genes (Figure 1C) (34). Our experiments did not indicate epistatic interaction between *KIAA0586* and *KIF7*, and a secondary occult mutation in either gene cannot be excluded. The c.428delG mutation results in a premature termination codon in five human *KIAA0586* isoforms, causing either a major protein truncation 5' to the essential coiled coil

560 domain, or NMD. It is comparable to the *talpid*^{3} chicken loss-of-function mutation which
561 introduces a frameshift in the orthologous region (Figure 1E). The c.428delG mutation is
562 annotated in dbSNP (rs534542684), and its MAF in the general population is surprisingly
563 high (0.39%, 378 out of 96534 alleles in the ExAC db), reminiscent of the most common
564 deafness (c.35delG in *GJB2*; 0,60% in the ExAC database) or cystic fibrosis (p.Phe508del in
565 *CFTR*; 0.67% in the ExAC database) mutation. In two concurrent studies reporting
566 *KIAA0586* mutations in JBTS patients, c.428delG represented the most prevalent mutation
567 (43, 44). While c.428delG was clearly enriched in patients with biallelic *KIAA0586* mutations
568 in both studies (present in 20 of 24 such patients), only two were homozygous. Despite its
569 commonness, c.428delG was neither observed in homozygous state in healthy individuals in
570 the TGP, ESP, or ExAC databases. Such rarity of homozygosity could indicate that it causes
571 embryonic lethality, early death or severe illness leading to underrepresentation of the
572 respective samples. Embryonic lethality in *talpid*^{3} chicken and *Talpid3*$^{-/-}$ knockout mice
573 would support such an interpretation. On the other hand, c.428delG was not found in a
574 simultaneous study that reports biallelic *KIAA0586* mutations in early lethal ciliopathies (47).
575 Of note, a very recent study on rare human knockouts identified in the genomes of 2,636
576 healthy Icelanders lists one individual of 57 years with homozygosity for c.428delG (48).
577 This could either be due to protective modifiers or a low mutational load in the ciliome of the
578 respective person. Assuming the latter, c.428delG$_{KIAA0586}$ could represent a hypomorphic
579 allele that increases susceptibility to develop JBTS, with more severe mutations required
580 either *in trans* (in heterozygous carriers, as in most patients reported by Roosing et al. and
581 Bachmann-Gagescu et al. (43, 44)), or in other genes (in homozygous carriers) for disease
582 manifestation. The presence of a heterozygous potentially deleterious *C5orf42* (*JBTS17*)
583 variant in the only c.428delG$_{KIAA0586}$-homozygous patient reported by Bachmann-Gagescu et
584 al. (44), and the co-occurence of such variants in four ciliopathy genes in patient G2

585 (including a truncation in the JBTS gene *KIF7*) support the categorization of
586 c.428delG$_{KIAA0586}$ as a hypomorphic mutation of incomplete penetrance. Of note, no
587 secondary *KIAA0586* mutation was identified in c.428delG-heterozygous JBTS patients in
588 the two other studies (43, 44), which could be due to the contribution of other genes.
589 The homozygous mutations c.2414-1G>C (Family 1) and c.2512C>T (p.Arg838*, Family 2),
590 would not disrupt the 5' functionally essential coiled coil domain in the consecutive
591 KIAA0586 protein, and partial function may be maintained (possibly due to preserved, albeit
592 truncated, KIAA0586 protein). We have shown that KIAA0586 has several functions in the
593 centriole, and this may be mediated by different protein residues.
594 The occurrence of retinal degeneration in JBTS depends on the genetic subtype, but is
595 variable even within a family. The localization of KIAA0586 at the ciliary base of retinal
596 photoreceptor cells corresponds to other JBTS proteins. Proteins of the periciliary
597 compartment at the base of the photoreceptor cilium are thought to be critical for the
598 handover of cargo from the dynein-mediated transport through the inner segment to the
599 kinesin-powered anterograde intraflagellar transport in the ciliary compartment (33, 49).
600 KIAA0586 may be part of the protein networks implicated in these processes. The lack of
601 retinal disease in the patients described herein may be due to the less strongly developed
602 structure of the distal appendages and/or the possible functional redundancy in the cilia of
603 retinal photoreceptor cells. Nevertheless, patients with *KIAA0586*-related JBTS should be
604 investigated for signs of retinal degeneration, and given that mutations in the JBTS gene
605 *CEP290* may cause non-syndromic Leber congenital amaurosis (50), *KIAA0586* represents a
606 candidate gene for isolated retinopathies.
607 Loss of KIAA0586 (TALPID3) function in animal models results in a failure to produce both
608 primary and motile cilia. Previously it has been suggested that this is due to a failure of the
609 centrosome to migrate apically or dock at the plasma membrane (7, 12). The subsequent

failure of cilia formation results in abnormal Hh signaling and disrupted GLI processing (11). Most patients with *KIAA0586*-related JBTS exhibit few classical Hh phenotypes such as polydactyly (this study, (43, 44)), unlike the corresponding mouse, chicken and zebrafish models (6, 10, 11). We show that, independent of Hh signaling, cell and tissue polarity are disrupted upon loss of *TALPID3*. JBTS is characterized by cerebellar hypoplasia and loss of decussation of neuronal projections from the cerebellum (1). While Hh signalling is required for controlling the growth of the embryonic cerebellar primordia (51), the failure of decussation has been proposed to result from defective axonal guidance (1), a process depending on centrosome-guided cell polarity (52). Furthermore, we have shown that in inner ear HCs, cell polarity and ciliogenesis, albeit closely linked, are differentially affected in *talpid*^{3} cells. Thus, loss of decussation may reflect loss of polarity.

We propose that KIAA0586 exerts a role in intracellular trafficking and cell polarity distinct from its role in docking of the centriole. *Talpid*^{3} cells have abnormal microtubule dynamics (7). Microtubules are required for the recruitment of satellites and proteins in the distal centriole (53, 54), a process known to be impaired by loss of KIAA0586. Abnormal cell polarity in *talpid*^{3} cells may be due to the effect of TALPID3 on microtubule dynamics and a direct role in centrosome organization: Microtubules are essential for intracellular trafficking, cellular structure and polarity. We have shown that localization of the centrosome, mitochondria and Golgi is disrupted in *talpid*^{3} cells. Moreover, Rab8, a GTPase which binds to the Golgi and is required for vesicular trafficking and ciliogenesis (55-57), is mislocalized in *KIAA0586*-depleted cells (9). In JBTS patients with mutations in *AHI1* (*JBTS3*), encoding an interactor of RAB8 (58), non-ciliary trafficking from the Golgi and ciliogenesis are impaired. Of note, Golgi mislocalization in the *talpid*^{3} choroid plexus is similar to what has been observed in *Ahi1*$^{-/-}$ mice (58). This suggests a similar pathogenesis of *JBTS23* and *JBTS3*, with defective cell polarity, intracellular trafficking, and Hh signaling.

635 KIAA0586 interacts with CP110 and Cep120 (9), distal centriolar proteins implicated in
636 centriole duplication and maturation, and ciliogenesis. The predominant expression of
637 Cep120 on the daughter centriole throughout most of the cell cycle depends on Kiaa0586, as
638 indicated by high expression of Cep120 on both centrioles and absence of CP110 from the
639 mother centriole prior to ciliogenesis in *Talpid3*$^{-/-}$ cells (59). Although equal expression of
640 KIAA0586 on the mother and daughter centrioles has been reported (this study, (9)) there is
641 evidence that KIAA0586 predominantly localizes at the mother centriole (8). In addition, loss
642 of chicken *KIAA0586* (*TALPID3*) causes centriole elongation whereas overexpression of
643 Cep120 causes elongation of the mother centriole, suggesting that KIAA0586 (TALPID3)
644 may control centriole length through depletion or suppression of Cep120 on the mother
645 centriole. Similarly, depletion of CP110 also increases centriole length (53), suggesting that
646 KIAA0586 regulates centriolar length through controling CP110 localization and centriolar
647 capping of the distal mother centriole. Loss of other centriolar proteins, such as OFD1,
648 likewise results in elongated centrioles and loss of distal appendages (60). Based on the
649 colocalization of KIAA0586, CP110 and Cep164, it has been proposed that KIAA0586
650 regulates ciliary vesicle docking adjacent to Cep164 localization (9), but not distal appendage
651 formation itself, and this is supported by evidence from human patient *KIAA0586*$^{-/-}$ cells
652 which show Cep164 within the distal centriole (46). We also find evidence for a vesicle
653 docking defect, demonstrated by an increase in centriolar satellites. However, we propose
654 that *KIAA0586* loss primarily causes abnormal distal appendages and impaired Cep164
655 localization, similar to what can be observed in OFD1 mutants (60). In addition,
656 determination of Cep164 expression in cells of highly polarized tissue demonstrates a further
657 centriolar defect not easily distinguished in *in vitro* assays – the loss of centriole orientation
658 to the apical membrane of the cell. Whether this defect is due to the depletion of KIAA0586

659 from the centriole or impairment of another function of KIAA0586 in pericentriolar regions
660 or cytoskeleton remains to be elucidated.
661 We have identified *KIAA0586* as a novel gene for JBTS, and we propose that it is not only
662 required for ciliogenesis, but also to establish cell and thus tissue polarity. *JBTS23*, and
663 possibly other JBTS subtypes, may result from impairment of both functions.
664

665 **ACKNOWLEGMENTS**

666 We are indebted to the families who participated in our study. We thank Prof. Chi-chung Hui,
667 Department of Molecular Genetics, University of Toronto, for the kind gift of the *Kif7* mouse
668 line, Prof. Andrew Forge for help with basal papilla dissection, John James, CHIPs,
669 University of Dundee, UK, Maurits Jansen of Edinburgh Preclinical Imaging,
670 University/BHF Centre for Cardiovascular Science, University of Edinburgh for technical
671 help, ESRIC for support with advanced imaging, Dr Denis Headon for the kind gift of the β-
672 catenin probe and Dr Jeremy Reiter for the kind gift of the Azi1 antibody. We thank
673 Elisabeth Sehn, and Gabi Stern-Schneider (both JGU Mainz) for their skillful technical
674 assistance.
675 Conflict of Interest Statement: H.J.B. is employee of Bioscientia which is part of a publicly
676 traded diagnostic company. The work described in this study is unrelated to this employment.
677 The other authors have no competing interests.
678

679 **Funding**

680 MGD, LAS, GMD and LM are supported by BBSRC Career Track Fellowship funding to
681 MGD (BB/F024347/1) and through funding to The Roslin Institute via Institute Strategic
682 Grant funding from the BBSRC. AMF is funded by a BBSRC DTG EastBio Studentship.
683 UW was supported by European Community FP7/2009/241955 (SYSCILIA), FAUN-

Stiftung, Nuremberg, Foundation Fighting Blindness (FFB), and the BMBF "HOPE2" (01GM1108D). HJB was supported by funding from the Imhoff-Stiftung, Köln Fortune (University Hospital of Cologne), the Deutsche Heredo-Ataxie-Gesellschaft e.V., DHAG and Stiftung Auge (Deutsche Ophthalmologische Gesellschaft). RAJ was supported by the DFG (AB393/2-2).

691 **REFERENCES**

692 1. Romani M, Micalizzi A, Valente EM. Joubert syndrome: congenital cerebellar ataxia with the
693 molar tooth. Lancet Neurol. 2013 Sep;12(9):894-905. PubMed PMID: 23870701. Pubmed Central
694 PMCID: 3809058.
695 2. Bachmann-Gagescu R, Dempsey JC, Phelps IG, O'Roak BJ, Knutzen DM, Rue TC, et al. Joubert
696 syndrome: a model for untangling recessive disorders with extreme genetic heterogeneity. J Med
697 Genet. 2015 Jun 19. PubMed PMID: 26092869.
698 3. Christensen ST, Pedersen LB, Schneider L, Satir P. Sensory cilia and integration of signal
699 transduction in human health and disease. Traffic. 2007 Feb;8(2):97-109. PubMed PMID: 17241444.
700 4. Goetz SC, Anderson KV. The primary cilium: a signalling centre during vertebrate
701 development. Nat Rev Genet. 2010 May;11(5):331-44. PubMed PMID: 20395968. Pubmed Central
702 PMCID: 3121168.
703 5. Bettencourt-Dias M, Hildebrandt F, Pellman D, Woods G, Godinho SA. Centrosomes and cilia
704 in human disease. Trends Genet. 2011 Aug;27(8):307-15. PubMed PMID: 21680046. Pubmed Central
705 PMCID: 3144269.
706 6. Ben J, Elworthy S, Ng AS, van Eeden F, Ingham PW. Targeted mutation of the talpid3 gene in
707 zebrafish reveals its conserved requirement for ciliogenesis and Hedgehog signalling across the
708 vertebrates. Development. 2011 Nov;138(22):4969-78. PubMed PMID: 22028029. Pubmed Central
709 PMCID: 3201664.
710 7. Yin Y, Bangs F, Paton IR, Prescott A, James J, Davey MG, et al. The Talpid3 gene (KIAA0586)
711 encodes a centrosomal protein that is essential for primary cilia formation. Development. 2009
712 Feb;136(4):655-64. PubMed PMID: 19144723. Pubmed Central PMCID: 2741201.
713 8. Wu C, Yang M, Li J, Wang C, Cao T, Tao K, et al. Talpid3-binding centrosomal protein Cep120
714 is required for centriole duplication and proliferation of cerebellar granule neuron progenitors. PLoS
715 One. 2014;9(9):e107943. PubMed PMID: 25251415. Pubmed Central PMCID: 4176001.
716 9. Kobayashi T, Kim S, Lin YC, Inoue T, Dynlacht BD. The CP110-interacting proteins Talpid3 and
717 Cep290 play overlapping and distinct roles in cilia assembly. J Cell Biol. 2014 Jan 20;204(2):215-29.
718 PubMed PMID: 24421332. Pubmed Central PMCID: 3897186.
719 10. Bangs F, Antonio N, Thongnuek P, Welten M, Davey MG, Briscoe J, et al. Generation of mice
720 with functional inactivation of talpid3, a gene first identified in chicken. Development. 2011
721 Aug;138(15):3261-72. PubMed PMID: 21750036. Pubmed Central PMCID: 3133916.
722 11. Davey MG, Paton IR, Yin Y, Schmidt M, Bangs FK, Morrice DR, et al. The chicken talpid3 gene
723 encodes a novel protein essential for Hedgehog signaling. Genes Dev. 2006 May 15;20(10):1365-77.
724 PubMed PMID: 16702409. Pubmed Central PMCID: 1472910.
725 12. Stephen LA, Davis GM, McTeir KE, James J, McTeir L, Kierans M, et al. Failure of centrosome
726 migration causes a loss of motile cilia in talpid(3) mutants. Dev Dyn. 2013 Aug;242(8):923-31.
727 PubMed PMID: 23613203.
728 13. Tsang WY, Dynlacht BD. CP110 and its network of partners coordinately regulate cilia
729 assembly. Cilia. 2013;2(1):9. PubMed PMID: 24053599. Pubmed Central PMCID: 3744162.
730 14. Fu W, O'Connor TD, Jun G, Kang HM, Abecasis G, Leal SM, et al. Analysis of 6,515 exomes
731 reveals the recent origin of most human protein-coding variants. Nature. 2013 Jan
732 10;493(7431):216-20. PubMed PMID: 23201682. Pubmed Central PMCID: 3676746.
733 15. Via M, Gignoux C, Burchard EG. The 1000 Genomes Project: new opportunities for research
734 and social challenges. Genome Med. 2010;2(1):3. PubMed PMID: 20193048. Pubmed Central PMCID:
735 2829928.
736 16. Abou Jamra R, Wohlfart S, Zweier M, Uebe S, Priebe L, Ekici A, et al. Homozygosity mapping
737 in 64 Syrian consanguineous families with non-specific intellectual disability reveals 11 novel loci and
738 high heterogeneity. Eur J Hum Genet. 2011 Nov;19(11):1161-6. PubMed PMID: 21629298. Pubmed
739 Central PMCID: 3198153.

17. Abou Jamra R, Philippe O, Raas-Rothschild A, Eck SH, Graf E, Buchert R, et al. Adaptor protein complex 4 deficiency causes severe autosomal-recessive intellectual disability, progressive spastic paraplegia, shy character, and short stature. Am J Hum Genet. 2011 Jun 10;88(6):788-95. PubMed PMID: 21620353. Pubmed Central PMCID: 3113253.
18. Riecken LB, Tawamie H, Dornblut C, Buchert R, Ismayel A, Schulz A, et al. Inhibition of RAS activation due to a homozygous ezrin variant in patients with profound intellectual disability. Hum Mutat. 2015 Feb;36(2):270-8. PubMed PMID: 25504542.
19. Ahmed I, Buchert R, Zhou M, Jiao X, Mittal K, Sheikh TI, et al. Mutations in DCPS and EDC3 in autosomal recessive intellectual disability indicate a crucial role for mRNA decapping in neurodevelopment. Hum Mol Genet. 2015 Feb 20. PubMed PMID: 25701870.
20. Basmanav FB, Oprisoreanu AM, Pasternack SM, Thiele H, Fritz G, Wenzel J, et al. Mutations in POGLUT1, encoding protein O-glucosyltransferase 1, cause autosomal-dominant Dowling-Degos disease. Am J Hum Genet. 2014 Jan 2;94(1):135-43. PubMed PMID: 24387993. Pubmed Central PMCID: 3882728.
21. Beck BB, Phillips JB, Bartram MP, Wegner J, Thoenes M, Pannes A, et al. Mutation of POC1B in a severe syndromic retinal ciliopathy. Hum Mutat. 2014 Oct;35(10):1153-62. PubMed PMID: 25044745.
22. Cheung HO, Zhang X, Ribeiro A, Mo R, Makino S, Puviindran V, et al. The kinesin protein Kif7 is a critical regulator of Gli transcription factors in mammalian hedgehog signaling. Sci Signal. 2009;2(76):ra29. PubMed PMID: 19549984.
23. Hamburger V, Hamilton HL. A series of normal stages in the development of the chick embryo. J Morphol. 1951 Jan;88(1):49-92. PubMed PMID: 24539719.
24. Davey MG, McTeir L, Barrie AM, Freem LJ, Stephen LA. Loss of cilia causes embryonic lung hypoplasia, liver fibrosis, and cholestasis in the talpid3 ciliopathy mutant. Organogenesis. 2014 Apr-Jun;10(2):177-85. PubMed PMID: 24743779. Pubmed Central PMCID: 4154951.
25. Nieto MA, Patel K, Wilkinson DG. In situ hybridization analysis of chick embryos in whole mount and tissue sections. Methods Cell Biol. 1996;51:219-35. PubMed PMID: 8722478.
26. Das RM, Van Hateren NJ, Howell GR, Farrell ER, Bangs FK, Porteous VC, et al. A robust system for RNA interference in the chicken using a modified microRNA operon. Dev Biol. 2006 Jun 15;294(2):554-63. PubMed PMID: 16574096.
27. Hall EA, Keighren M, Ford MJ, Davey T, Jarman AP, Smith LB, et al. Acute versus chronic loss of mammalian Azi1/Cep131 results in distinct ciliary phenotypes. PLoS Genet. 2013;9(12):e1003928. PubMed PMID: 24415959. Pubmed Central PMCID: 3887133.
28. Overlack N, Kilic D, Bauss K, Marker T, Kremer H, van Wijk E, et al. Direct interaction of the Usher syndrome 1G protein SANS and myomegalin in the retina. Biochim Biophys Acta. 2011 Oct;1813(10):1883-92. PubMed PMID: 21767579.
29. Trojan P, Krauss N, Choe HW, Giessl A, Pulvermuller A, Wolfrum U. Centrins in retinal photoreceptor cells: regulators in the connecting cilium. Prog Retin Eye Res. 2008 May;27(3):237-59. PubMed PMID: 18329314.
30. Davey MG, James J, Paton IR, Burt DW, Tickle C. Analysis of talpid3 and wild-type chicken embryos reveals roles for Hedgehog signalling in development of the limb bud vasculature. Dev Biol. 2007 Jan 1;301(1):155-65. PubMed PMID: 16959240.
31. Paintrand M, Moudjou M, Delacroix H, Bornens M. Centrosome organization and centriole architecture: their sensitivity to divalent cations. J Struct Biol. 1992 Mar-Apr;108(2):107-28. PubMed PMID: 1486002.
32. Maerker T, van Wijk E, Overlack N, Kersten FF, McGee J, Goldmann T, et al. A novel Usher protein network at the periciliary reloading point between molecular transport machineries in vertebrate photoreceptor cells. Hum Mol Genet. 2008 Jan 1;17(1):71-86. PubMed PMID: 17906286.
33. Sedmak T, Wolfrum U. Intraflagellar transport molecules in ciliary and nonciliary cells of the retina. J Cell Biol. 2010 Apr 5;189(1):171-86. PubMed PMID: 20368623. Pubmed Central PMCID: 2854383.

34. Dafinger C, Liebau MC, Elsayed SM, Hellenbroich Y, Boltshauser E, Korenke GC, et al. Mutations in KIF7 link Joubert syndrome with Sonic Hedgehog signaling and microtubule dynamics. J Clin Invest. 2011 Jul;121(7):2662-7. PubMed PMID: 21633164. Pubmed Central PMCID: 3223820.
35. Lee JE, Silhavy JL, Zaki MS, Schroth J, Bielas SL, Marsh SE, et al. CEP41 is mutated in Joubert syndrome and is required for tubulin glutamylation at the cilium. Nat Genet. 2012 Feb;44(2):193-9. PubMed PMID: 22246503. Pubmed Central PMCID: 3267856.
36. Filges I, Nosova E, Bruder E, Tercanli S, Townsend K, Gibson WT, et al. Exome sequencing identifies mutations in KIF14 as a novel cause of an autosomal recessive lethal fetal ciliopathy phenotype. Clin Genet. 2014 Sep;86(3):220-8. PubMed PMID: 24128419.
37. Kim SK, Shindo A, Park TJ, Oh EC, Ghosh S, Gray RS, et al. Planar cell polarity acts through septins to control collective cell movement and ciliogenesis. Science. 2010 Sep 10;329(5997):1337-40. PubMed PMID: 20671153. Pubmed Central PMCID: 3509789.
38. Kim J, Lee JE, Heynen-Genel S, Suyama E, Ono K, Lee K, et al. Functional genomic screen for modulators of ciliogenesis and cilium length. Nature. 2010 Apr 15;464(7291):1048-51. PubMed PMID: 20393563. Pubmed Central PMCID: 2929961.
39. Happe H, de Heer E, Peters DJ. Polycystic kidney disease: the complexity of planar cell polarity and signaling during tissue regeneration and cyst formation. Biochim Biophys Acta. 2011 Oct;1812(10):1249-55. PubMed PMID: 21640821.
40. Carroll TJ, Yu J. The kidney and planar cell polarity. Curr Top Dev Biol. 2012;101:185-212. PubMed PMID: 23140630.
41. Tarchini B, Jolicoeur C, Cayouette M. A molecular blueprint at the apical surface establishes planar asymmetry in cochlear hair cells. Dev Cell. 2013 Oct 14;27(1):88-102. PubMed PMID: 24135232.
42. Andersen JS, Wilkinson CJ, Mayor T, Mortensen P, Nigg EA, Mann M. Proteomic characterization of the human centrosome by protein correlation profiling. Nature. 2003 Dec 4;426(6966):570-4. PubMed PMID: 14654843.
43. Roosing S, Hofree M, Kim S, Scott E, Copeland B, Romani M, et al. Functional genome-wide siRNA screen identifies KIAA0586 as mutated in Joubert syndrome. Elife. 2015;4. PubMed PMID: 26026149. Pubmed Central PMCID: 4477441.
44. Bachmann-Gagescu R, Phelps IG, Dempsey JC, Sharma VA, Ishak GE, Boyle EA, et al. KIAA0586 is Mutated in Joubert Syndrome. Hum Mutat. 2015 Jun 11. PubMed PMID: 26096313.
45. Lewis KE, Drossopoulou G, Paton IR, Morrice DR, Robertson KE, Burt DW, et al. Expression of ptc and gli genes in talpid3 suggests bifurcation in Shh pathway. Development. 1999 Jun;126(11):2397-407. PubMed PMID: 10225999.
46. Buxton P, Davey MG, Paton IR, Morrice DR, Francis-West PH, Burt DW, et al. Craniofacial development in the talpid3 chicken mutant. Differentiation. 2004 Sep;72(7):348-62. PubMed PMID: 15554946.
47. Alby C, Piquand K, Huber C, Megarbane A, Ichkou A, Legendre M, et al. Mutations in KIAA0586 Cause Lethal Ciliopathies Ranging from a Hydrolethalus Phenotype to Short-Rib Polydactyly Syndrome. Am J Hum Genet. 2015 Jul 7. PubMed PMID: 26166481.
48. Sulem P, Helgason H, Oddson A, Stefansson H, Gudjonsson SA, Zink F, et al. Identification of a large set of rare complete human knockouts. Nat Genet. 2015 Mar 25. PubMed PMID: 25807282.
49. Roepman R, Wolfrum U. Protein networks and complexes in photoreceptor cilia. Subcell Biochem. 2007;43:209-35. PubMed PMID: 17953396.
50. den Hollander AI, Koenekoop RK, Yzer S, Lopez I, Arends ML, Voesenek KE, et al. Mutations in the CEP290 (NPHP6) gene are a frequent cause of Leber congenital amaurosis. Am J Hum Genet. 2006 Sep;79(3):556-61. PubMed PMID: 16909394. Pubmed Central PMCID: 1559533.
51. Lewis PM, Gritli-Linde A, Smeyne R, Kottmann A, McMahon AP. Sonic hedgehog signaling is required for expansion of granule neuron precursors and patterning of the mouse cerebellum. Dev Biol. 2004 Jun 15;270(2):393-410. PubMed PMID: 15183722.

841 52. Solecki DJ, Govek EE, Tomoda T, Hatten ME. Neuronal polarity in CNS development. Genes
842 Dev. 2006 Oct 1;20(19):2639-47. PubMed PMID: 17015428.
843 53. Schmidt TI, Kleylein-Sohn J, Westendorf J, Le Clech M, Lavoie SB, Stierhof YD, et al. Control of
844 centriole length by CPAP and CP110. Curr Biol. 2009 Jun 23;19(12):1005-11. PubMed PMID:
845 19481458.
846 54. Kim J, Krishnaswami SR, Gleeson JG. CEP290 interacts with the centriolar satellite
847 component PCM-1 and is required for Rab8 localization to the primary cilium. Hum Mol Genet. 2008
848 Dec 1;17(23):3796-805. PubMed PMID: 18772192. Pubmed Central PMCID: 2722899.
849 55. Nachury MV, Loktev AV, Zhang Q, Westlake CJ, Peranen J, Merdes A, et al. A core complex of
850 BBS proteins cooperates with the GTPase Rab8 to promote ciliary membrane biogenesis. Cell. 2007
851 Jun 15;129(6):1201-13. PubMed PMID: 17574030.
852 56. Feng S, Knodler A, Ren J, Zhang J, Zhang X, Hong Y, et al. A Rab8 guanine nucleotide
853 exchange factor-effector interaction network regulates primary ciliogenesis. J Biol Chem. 2012 May
854 4;287(19):15602-9. PubMed PMID: 22433857. Pubmed Central PMCID: 3346093.
855 57. Henry L, Sheff DR. Rab8 regulates basolateral secretory, but not recycling, traffic at the
856 recycling endosome. Mol Biol Cell. 2008 May;19(5):2059-68. PubMed PMID: 18287531. Pubmed
857 Central PMCID: 2366880.
858 58. Hsiao YC, Tong ZJ, Westfall JE, Ault JG, Page-McCaw PS, Ferland RJ. Ahi1, whose human
859 ortholog is mutated in Joubert syndrome, is required for Rab8a localization, ciliogenesis and vesicle
860 trafficking. Hum Mol Genet. 2009 Oct 15;18(20):3926-41. PubMed PMID: 19625297. Pubmed Central
861 PMCID: 2748898.
862 59. Spektor A, Tsang WY, Khoo D, Dynlacht BD. Cep97 and CP110 suppress a cilia assembly
863 program. Cell. 2007 Aug 24;130(4):678-90. PubMed PMID: 17719545.
864 60. Singla V, Romaguera-Ros M, Garcia-Verdugo JM, Reiter JF. Ofd1, a human disease gene,
865 regulates the length and distal structure of centrioles. Dev Cell. 2010 Mar 16;18(3):410-24. PubMed
866 PMID: 20230748. Pubmed Central PMCID: 2841064.
867 61. Liem KF, Jr., He M, Ocbina PJ, Anderson KV. Mouse Kif7/Costal2 is a cilia-associated protein
868 that regulates Sonic hedgehog signaling. Proc Natl Acad Sci U S A. 2009 Aug 11;106(32):13377-82.
869 PubMed PMID: 19666503. Pubmed Central PMCID: 2726420.

870

871

872

LEGENDS TO THE FIGURES

FIGURE 1

Patients with Joubert syndrome (JBTS) and *KIAA0586* mutations (A – C). (WT, wildtype; M, mutation). The "molar tooth sign" in cranial axial MRI is indicated by arrows. **A** Family 1. Homozygosity mapping yielded eight homozygous chromosomal candidate regions (not shown), including the *JBTS23* locus comprising *KIAA0586*. Patients MR026-01 and MR026-04 carry a homozygous splice site mutation, c.2414-1G>C. **B** Patient MD1 of Family 2 is compound heterozygous for two truncating mutations, including the prevalent c.428delG (p.Arg143Lysfs*4) allele. **C** Family 3: Patient G2 is double heterozygous for c.428delG in *KIAA0586*, and a frameshift mutation in *KIF7* (*JBTS12*; c.811delG, p.Glu271Argfs*51). He also carries three potentially pathogenic variants in the ciliopathy genes *CEP41*, *KIF14* and *WDPCP* (blue). **D** Genomic structure of *KIAA0586* with mutations in exons 5 and in/adjacent to exon 18 indicated. The gel electrophoresis shows the aberrant transcripts due to c.2414-1G>C. **E** Scheme of human KIAA0586 protein and predicted consequences of JBTS-associated mutations. Orange colour: unrelated residues included due to frameshift mutations. The 3rd coiled coil domain is the counterpart of the functionally essential 4th coiled coil domain in chicken (framed in red). **F** Chicken KIAA0586 is highly similar to the human protein. The *talpid*^{3} mutation results in an early frameshift and loss of three coiled coil domains, including the 4th one. The in-frame deletion of exons 11 and 12 of mouse *KIAA0586* (*2700049A03Rik*) is depicted above the scheme of the chicken ortholog.

FIGURE 2

Localization of KIAA0586 in primary cilia and in photoreceptor cilia of mammalian retinas. A Triple labeling of a ciliated IMCD3 cell demonstrates localization of Talpid3 (green) in the basal body (BB) and the adjacent centriole (Ce) at the base of the primary cilium co-stained by antibodies against Pericentrin-2 (PCNT2, red) and anti-acetylated tubulin (acTub, cyan), a biomarker of the axoneme (Ax). **B** Longitudinal cryosections through a mouse retina stained for Talpid3 (green) and

counterstained for the ciliary marker Centrin-3 (Cen3, red) and for the nuclear DNA marker DAPI reveal Talpid3 localization in the ciliary region (CR) at the joint between the inner (IS) and the outer segment (OS) of the photoreceptor layer, the outer (OPL) and inner inner plexiform layer (IPL). Overlay of DIC (differential interference contrast) image with DAPI (blue) nuclear stain in the outer (ONL) and the inner nuclear layer (INL) and in the ganglion cell layer (GC). **C-F** Immunostaining of cryosections through the photoreceptor layer of a mouse (**C**) and a human retina (**E**) demonstrate co-localization of KIAA0586 and Cen3 in the CR of photoreceptor cells. Higher magnification of double labeled mouse (**D**) and human (**F**) photoreceptor cilium reveals substantial localization of Talpid3/KIAA0586 at the centriole (Ce), the BB and between the Ce and BB of the photoreceptor cilium, but not in the connecting cilium (CC). **G, H** Immunoelectron microscopy analysis of longitudinal section through the cilium of a mouse rod photoreceptor cell and (**G**) higher magnification of the ciliary base (**H**) labeled for Talpid3 reveals Talpid3 in the periciliary region namely in the Ce and BB. **J** Schematic representation of Talpid3/KIAA0586 localization in the photoreceptor cilium. Scale bars: A, 1 μm; B, 10 μm; C, E, 5 μm; D, F, 0.5 μm; G, H, 200 nm.

FIGURE 3

Loss of *TALPID3* (*KIAA0586*) causes abnormal tissue and cell polarity and abnormal intracellular organization. A-B *β-catenin* expression is localized anteriorly within feather buds of the *wildtype* chicken at day 9.5. Black circles indicate featherbuds with correct polarity; dashed black circles represent no polarity; blue circles represent abnormal polarity (Schematic **C**) in the *talpid*^{3} chicken (**B''**) not seen in the *wildtype* chicken (**A''**). Asterisks represent merged feather buds. **D,E** SEM of the basilar papilla in *wildtype* (**D**) and *talpid*^{3} (**E**) chickens. Arrows indicate cilia. Curved lines represent the base of stereocilia hair bundles. **F-K** Actin bundles identified by phalloidin (green) and centriolar localization identified by γ tubulin (red). **F,G** Red circles with line represent orientation of polarized actin bundles in basilar papilla; dashed red circles represent unpolarized actin bundles (Schematic **L,M**). **H-K** Dashed white circles represent magnified images (**Ji-Kii'**). **Ji-Kii** White arrows indicate aligned centrosomes; blue arrows indicate unaligned centrosomes (Schematic **N**). **O,P**

Orientation based on placement of Golgi (TGN46, red) in comparison to actin indicating the leading edge (phalloidin, green) and nucleus (Dapi, blue, schematic in **Q**) in MEFs. Asterisks represent areas of higher magnification (not all represented at lower magnification). Scale Bars: A,B 5mm; A',A'',B',B'' 1 mm; D,E 1 μm; F,G,H,I,J,K 20 μm; F',G' 100 nm; Ji,Ji',Jii,Jii',Ki,Ki',Kii,Kii' 10 μm; O,P 100 μm; Oi,Oii,Oiii,Oiv,Ov,Ovi,Pi,Pii,Piii,Piv,Pv,Pvi 25 μm.

FIGURE 4

Loss of *TALPID3* causes abnormal intracellular organization and centriolar orientation

A,**B** The chicken choroid plexus at E8 is a highly polarized structure with docked centrioles (asterisk, **A**) identified within a clear centriolar zone apically (CZ, **A**) and a mitochondrial zone (MZ; m indicates mitochondria). The *talpid*^{3} choroid plexus (**B**) lacks these defined zones, with mitochondria identified in the most apical zone (m, **B**) centrioles identified throughout the cell, failing to dock (asterisk, **B**). Quantification of distance of mitochondria to cell surface (**C**). **D-G** *talpid*^{3} tissue is capable of producing mature centrioles. *Wildtype* centrioles (**D**) and *talpid*^{3} centrioles (**E,F**) exhibited subdistal appendages (SD), and distal appendages (DA), although DA were less frequently observed on *talpid*^{3} centrioles, quantified in (**G**). CEP164 localizes to the distal mother centriole in *wildtype* and *talpid*^{3} choroid plexus neuroepithelium (purple arrow indicated distal mother centriole, green arrow proximal centriole; **H,I,K,L**) and fibroblasts (**J,M**), but CEP164 puncta are smaller and disorganized in *talpid*^{3} choroid plexus and fail to orientate to the apical surface of the cell (arrows **L**). Centrioles in *wildtype* tissue were on average 0.7 μm (red line indicating centriole/basal body; **N,R**) compared to 0.9 μm in the *talpid*^{3} choroid plexus (**O,P,Q,R**). Scale bars: A,B=1μm, D,E,F=100 nm; H,K=10 μm I,J,L,M=5 μm, N,O,P,Q=200nm.

FIGURE 5

Analysis of centriolar satellites in the *talpid*^{3} choroid plexus. An area clear of electron-dense condensations was observed around the basal body in *wildtype* cells (area outlined by dots; **A**), electron-dense condensations were observed adjacent to *talpid*^{3} centrioles (indicated by arrows, **D**).

Quantified in (**G**). Immunostaining for a centriolar satellite marker in the choroid plexus, PCM1 (magnified area outlined by dashed line; PCM1=red, γ tubulin, green **B**, **C**, **E**, **F**). KIAA0586 protein does not colocalize with AZI1, a satellite protein in human RPE1 cells (KIAA0586=red, AZI1=green **H**, **J**). Scale bars: A,D=500 nm; B,E 10=μm;C,F= 2 μm H,I,K 5 μm.

Figure 1- figure supplement 1

Analysis of potential interactions between *Talpid3/TALPID3*, Kif7/*KIF7* and *IFT57* in the mouse and in chicken. Biallelic *KIF7* mutations cause JBTS type 12 in human (34). Although both the *KIAA0586* mutation c.428delG and the *KIF7* mutation c.811delG were paternally inherited in patient G2, we sought to test for subtle abnormalities resulting from this double heterozygosity. In addition, we had previously found through a microarray analysis of *talpid*^{3} limb buds that IFT57, a protein associated with ciliopathy phenotypes in mice and zebrafish, is downregulated in *talpid*^{3} embryos (10). Using *in ovo* complementation of the *talpid*^{3} neural tube, we could not detect induction of ISLET1 expression or ventralized PAX7 in the *wildtype* or *talpid*^{3} neural tube by overexpression of *KIF7* or *IFT57* (Figure SF1A,B). We then used siRNA constructs against *KIF7* to model a heterozygous loss of *KIF7* in the *TALPID3*$^{+/-}$ neural tube. Knock-down with two siRNA constructs had a weak effect on neural tube patterning compared to the mouse *KIF7*$^{-/-}$ knockout (22, 61). Although the NKX2.2 expression domain could be marginally expanded in *wildtype* embryos (not shown), there was no expansion of ISLET1 positive motorneuron progenitors in *wildtype* or *TALPID3*$^{+/-}$ embryos. PAX7, however, was weakly dorsalized in both *wildtype* and *talpid*$^{3+/-}$ embryos (Figure SF1C). These results suggested that some *KIF7* function may be cilia-independent as has been suggested (61). To more precisely investigate for a possible epistatic relationship between Kif7 and Talpid3, particularly in the organs primarily affected in JBTS, such as the cerebellum, we undertook a *Talpid3*$^{+/-}$ x *Kif7*$^{+/-}$ mouse cross in order to determine if double *Talpid3*$^{+/-}$/*Kif7*$^{+/-}$ heterozygous animals had brain patterning malformations. We first dissected embryos at E15.5, 16.5 and 17.5 and found that *Talpid3*$^{+/-}$/*Kif7*$^{+/-}$ embryos were morphologically normal, including size, situs and limb patterning. MEFs derived from E12.5 embryos were normally ciliated, with the percentage of ciliated

cells and cilia length comparable to those seen in *wildtype*, *Talpid3*$^{+/+}$*/Kif7*$^{+/-}$ and *Talpid3*$^{+/-}$*/Kif7*$^{+/+}$cells (Figure SF1F,G). MRI and sectioning of the brain also showed no brain patterning abnormalities (Figure SF1D,E). Subsequently *Talpid3*$^{+/-}$*/Kif7*$^{+/-}$ animals were born and grew normally compared to their litter mates and showed no abnormal brain morphology (Figure SF1). We conclude that *KIAA0586* (TALPID3) and *KIF7* do not act epistatically and hypothesize that additional genetic alterations in ciliopathy genes of patient G2, eventually including those identified in *CEP41* (*JBTS15*), *KIF14* and *WDPCP*, may contribute to a mutational load that is sufficient to elicit a JBTS phenotype on a *KIAA0586*$^{+/-}$*; KIF7*$^{+/-}$ background. **A** Overexpression of *IFT57* does not have an effect on patterning of the neural tube in the *talpid*^{3} chicken. **B** Overexpression of *KIF7* does not rescue or alter neural tube patterning in the *talpid*^{3} chicken. **C** siRNA knockdown of *KIF7* resulted in a weak dorsalization of *PAX7* but no expansion of *ISLET1*. **D** *Talpid3*$^{+/-}$*Kif7*$^{+/-}$ mice showed no gross anatomical abnormalities, neither were developmental brain defects identified through MRI (**D**) or histology (**E**). **F**, **G** No abnormalities were identified in either the percentage of ciliated cells (F), nor the length of cilia (**G**) in MEFs derived from wildtype, *Talpid3*$^{+/+}$*Kif7*$^{+/-}$, *Talpid3*$^{+/-}$*Kif7*$^{+/+}$ or *Talpid3*$^{+/-}$*Kif7*$^{+/-}$ mice.

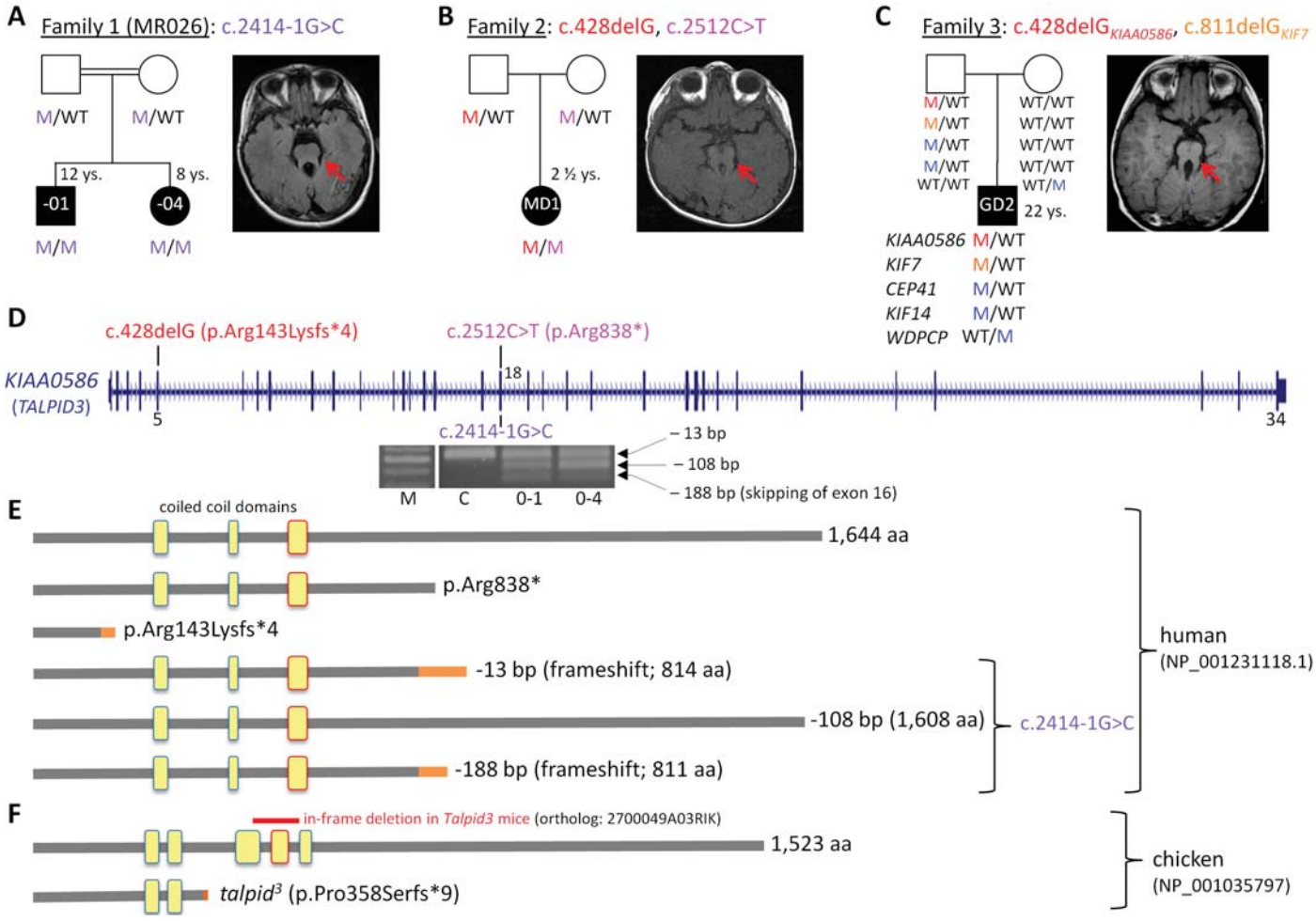
A
Family 1 (MR026): c.2414-1G>C
M/WT
M/WT
12 ys.
8 ys.
-01
-04
M/M
M/M
B
Family 2: c.428delG, c.2512C>T
M/WT
M/WT
2 ½ ys.
MD1
M/M
C
Family 3: c.428delG KIAA0586, c.811delG KIF7
M/WT
M/WT
M/WT
M/WT
WT/WT
WT/WT
WT/WT
WT/WT
WT/M
GD2
22 ys.
KIAA0586 M/WT
KIF7 M/WT
CEP41 M/WT
KIF14 M/WT
WDPCP WT/M
D
c.428delG (p.Arg143Lysfs*4)
c.2512C>T (p.Arg838*)
KIAA0586
(TALPID3)
5
18
34
c.2414-1G>C
– 13 bp
– 108 bp
– 188 bp (skipping of exon 16)
M
C
0-1
0-4
E
coiled coil domains
1,644 aa
p.Arg838*
p.Arg143Lysfs*4
-13 bp (frameshift; 814 aa)
-108 bp (1,608 aa)
-188 bp (frameshift; 811 aa)
c.2414-1G>C
human
(NP_001231118.1)
F
in-frame deletion in Talpid3 mice (ortholog: 2700049A03RIK)
1,523 aa
talpid3 (p.Pro358Serfs*9)
chicken
(NP_001035797)

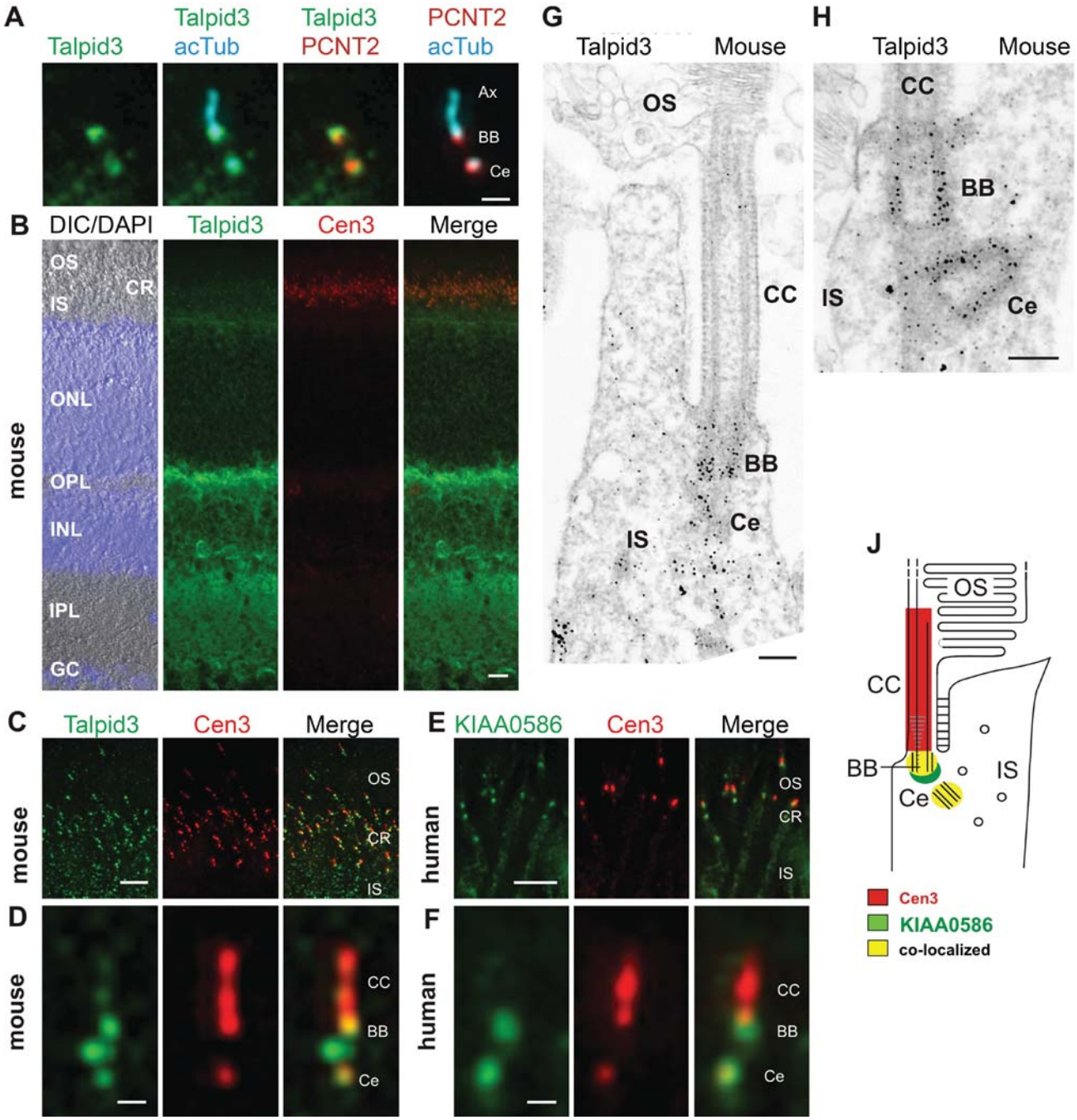
A
Talpid3
Talpid3
acTub
Talpid3
PCNT2
PCNT2
acTub
Ax
BB
Ce
B
DIC/DAPI
Talpid3
Cen3
Merge
mouse
OS
IS
CR
ONL
OPL
INL
IPL
GC
C
Talpid3
Cen3
Merge
mouse
OS
CR
IS
D
mouse
CC
BB
Ce
E
KIAA0586
Cen3
Merge
human
OS
CR
IS
F
human
CC
BB
Ce
G
Talpid3
Mouse
OS
CC
BB
Ce
IS
H
Talpid3
Mouse
CC
BB
IS
Ce
J
OS
CC
BB
IS
Ce
Cen3
KIAA0586
co-localized

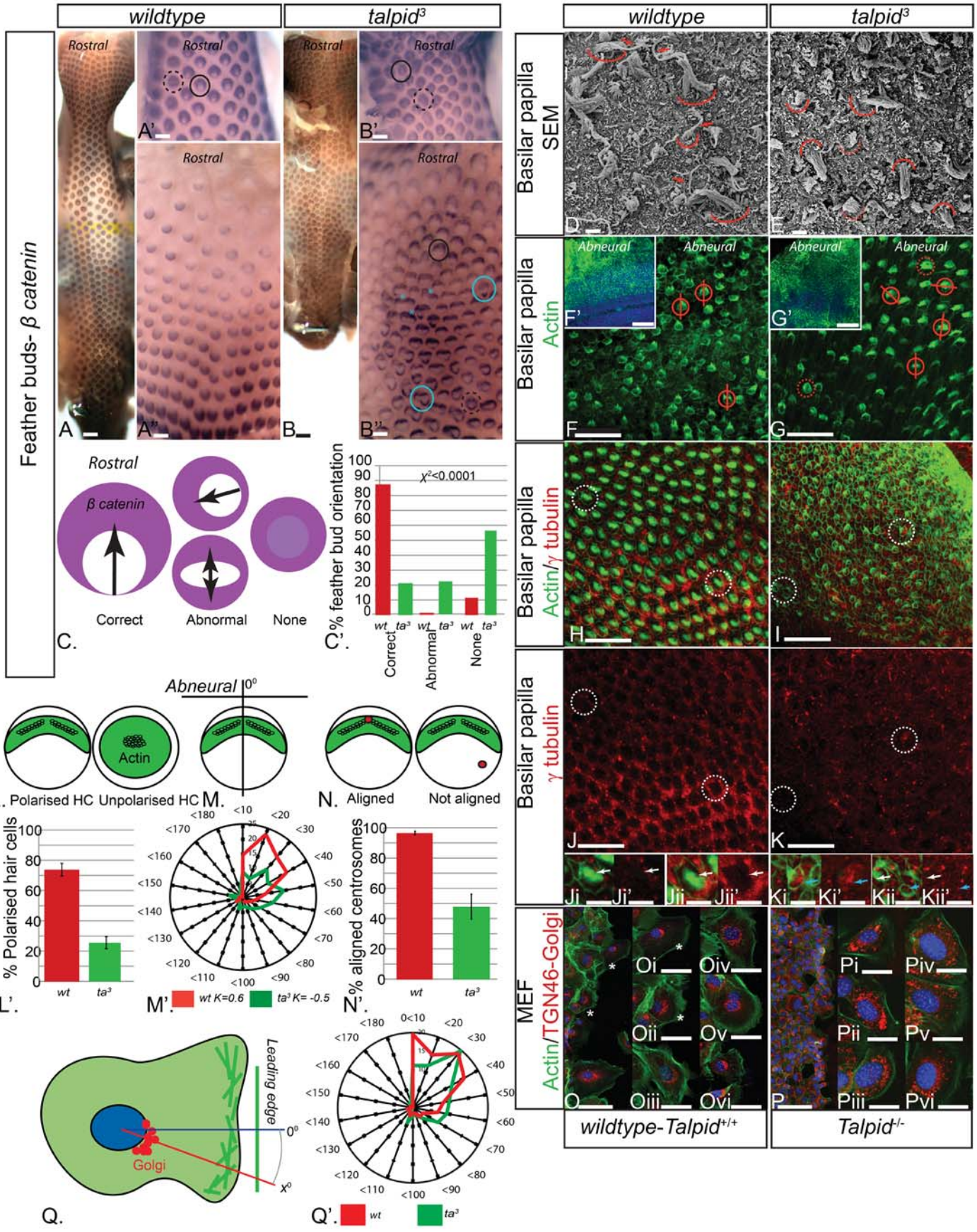
wildtype
talpid3
Feather buds- β catenin
Rostral
A
A'
A''
B
B'
B''
Rostral
β catenin
Correct
Abnormal
None
C.
C'.
% feather bud orientation
χ2<0.0001
wt
ta3
Abneural
Actin
L. Polarised HC
Unpolarised HC
M.
N. Aligned
Not aligned
% Polarised hair cells
L'.
M'.
wt K=0.6
ta3 K= -0.5
% aligned centrosomes
N'.
Leading edge
Golgi
Q.
Q'.
Basilar papilla SEM
Basilar papilla Actin
Basilar papilla Actin/γ tubulin
Basilar papilla γ tubulin
MEF Actin/TGN46-Golgi
wildtype-Talpid+/+
Talpid-/-

Figure 3

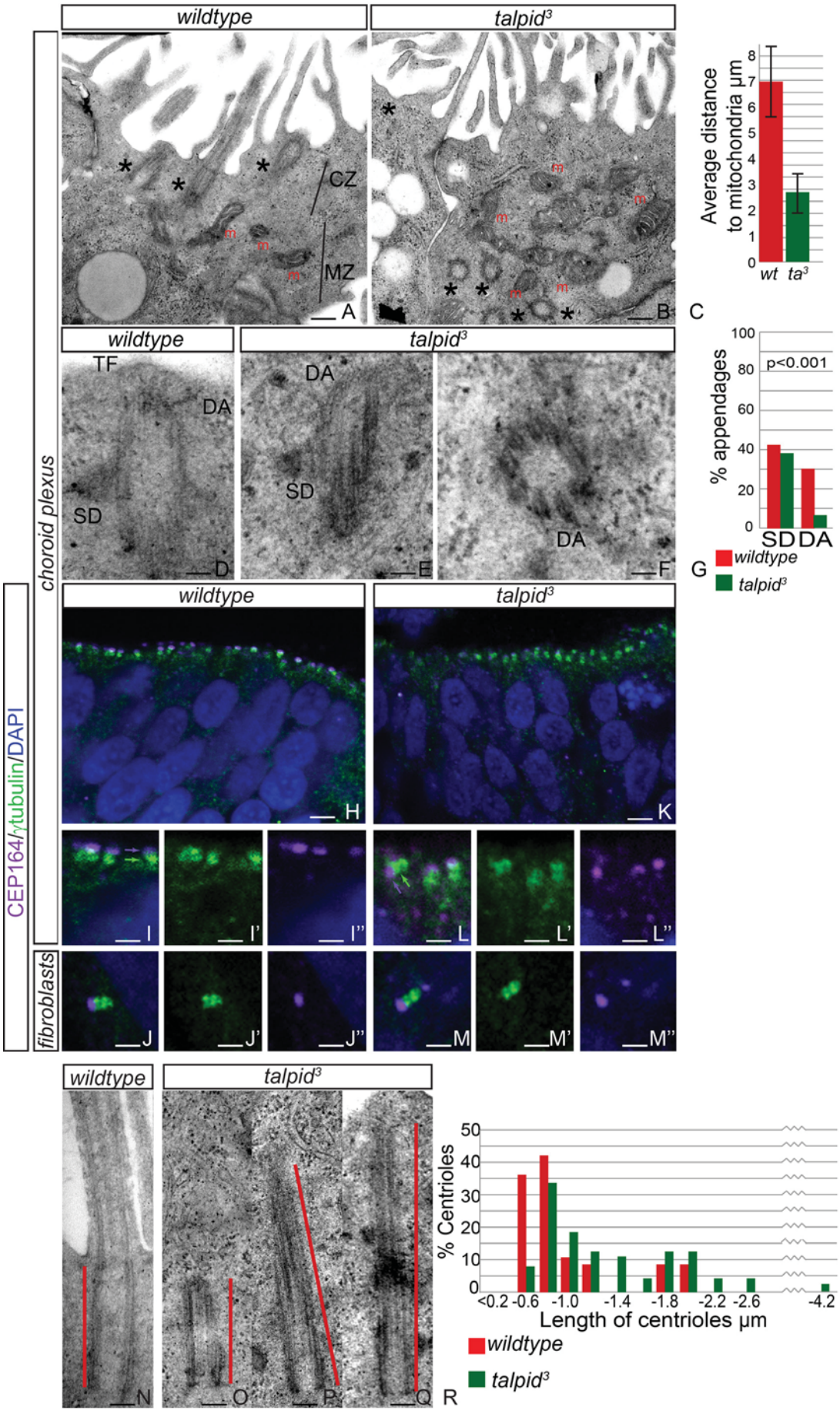
wildtype
talpid³
choroid plexus
CZ
MZ
m
A
B
Average distance to mitochondria µm
wt
ta³
C
TF
DA
SD
D
E
F
p<0.001
% appendages
SD DA
G
wildtype
talpid³
CEP164/γtubulin/DAPI
fibroblasts
H
K
I
I'
I''
L
L'
L''
J
J'
J''
M
M'
M''
N
O
P
Q
% Centrioles
<0.2 -0.6 -1.0 -1.4 -1.8 -2.2 -2.6 -4.2
Length of centrioles µm
R

Figure 4

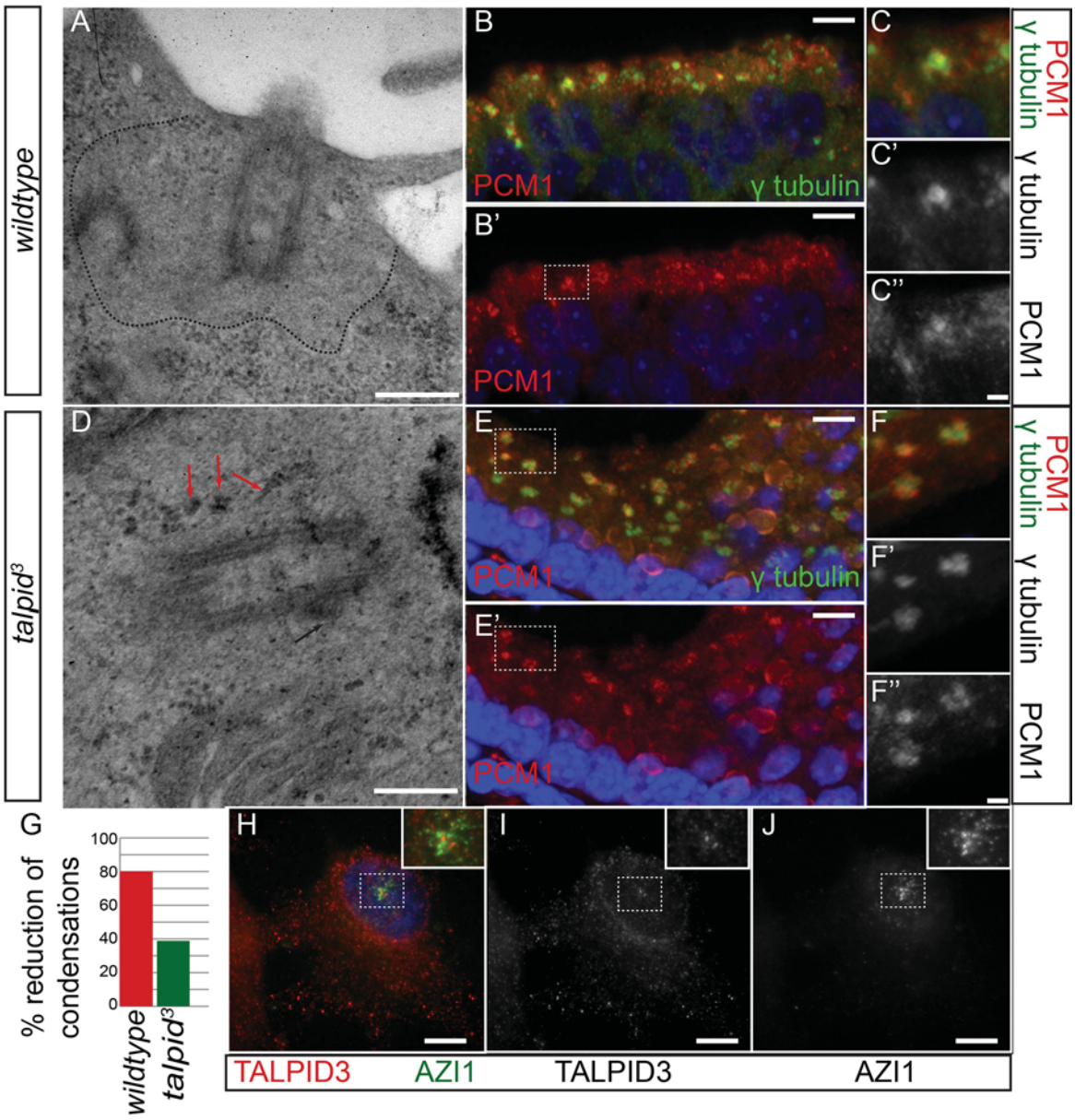
wildtype
talpid3
A
B
PCM1
γ tubulin
B'
C
C'
C''
PCM1
γ tubulin
PCM1
D
E
E'
F
F'
F''
G
% reduction of condensations
100
80
60
40
20
0
wildtype
talpid3
H
I
J
TALPID3
AZI1
TALPID3
AZI1

Figure 5